Enhancement of Bipartite Entanglement in Cavity Magnomechanical Systems Assisted by an Optical Parametric Amplifier

Amanuel Dereje Woldsenbet

A Thesis Submitted to the Department of Applied Physics

School of Applied Natural Science

Presented in Partial Fulfillment of the Requirement for the Degree of Master's in Applied Physics (Quantum Optics)

Office of Graduate Studies

Adama Science and Technology University

June, 2024

Adama, Ethiopia

Enhancement of Bipartite Entanglement in Cavity Magnomechanical Systems Assisted by an Optical Parametric Amplifier

Amanuel Dereje Woldsenbet

Advisor: Dr. Tewdros Yirgashewa

Co-advisor: Dr.Fekadu Tolessa

A Thesis Submitted to the Department of Applied Physics

School of Applied Natural Science

Presented in Partial Fulfillment of the Requirement for the Degree of Master's in Applied Physics (Quantum Optics)

Office of Graduate Studies

Adama Science and Technology University

June, 2024

Adama, Ethiopia

Declaration

I declare that this Master's thesis entitled *"***Enhancement of Bipartite Entanglement in Cavity Magnomechanical Systems Assisted by an Optical Parametric Amplifier***"* is my own work and has not been submitted to any university for a similar purpose. The references used in this thesis are duly recognized by proper citations.

Amanuel Dereje Woldsenbet	____________	____________
Name of student	Signature	Date

Recommendation

We,the advisors of this thesis, hereby certify that we have read the revised version of the thesis entitled "**Enhancement of Bipartite Entanglement in Cavity Magnomechanical Systems Assisted by an Optical Parametric Amplifier**" prepared under our guidance by Amanuel Dereje Woldsenbet submitted in partial fulfillment of the requirement for the degree of Master's of Science in Applied Physics. Therefore ,we recommend the submission of the revised version of the thesis to the department following the applicable procedures.

Dr. Tewdros Yirgashewa	____________	____________
Advisor	Signature	Date
Dr. Fekadu Tolessa	____________	____________
Co-advisor	Signature	Date

Approval Page

We, the undersigned, members of the Board of Examiners of the final open defense by **Amanuel Dereje Woldsenbet** have read and evaluated his thesis entitled "**Enhancement of Bipartite Entanglement in Cavity Magnomechanical Systems Assisted by an Optical Parametric Amplifier**"and examined the candidate. Therefore,this is to certify that the thesis has been accepted in partial fulfillment of the requirement of the degree of Master of Science in Applied Physics(Quantum Optics).

Chairperson	Signature	Date
Internal Examiner	Signature	Date
External Examiner	Signature	Date

Final approval and acceptance of the thesis is contingent upon submission of its final copy to the Office of Postgraduate Studies (OPGS) through the Department Graduate Council (DGC) and School Graduate Committee (SGC).

Department Head	Signature	Date
School Dean	Signature	Date
Office of Postgraduate Studies Dean	Signature	Date

Acknowledgement

First and foremost, I offer my profound gratitude and praises to God Almighty for His limitless blessings. I am deeply indebted to Dr. Tewodros Yirgashewa for his exceptional guidance and unwavering support during my academic journey. His vast knowledge and deep expertise have been instrumental in developing my understanding in this complex field, building a strong academic base. Additionally, I extend my heartfelt thanks to my co-advisor, Dr. Fekadu Tolessa, for his priceless advice and support.

I would also like to express my sincere appreciation to Adama Science and Technology University for providing the resources and environment that have greatly contributed to my research and academic growth. The facilities, staff, and vibrant academic community have been nothing short of inspiring.

List of Abbreviations

CM	Covariance Matrix
CMM	Cavity Magno Mechanical
cQED	cavity Quantum Electro Dynamics
CV	Continuous Variable
MW	Micro Wave
QLEs	Quantum Langevin Equations
YIG	Yttrium Iron Garnet
OPA	Optical Parametric Amplifier

List of Figures

Abstract

In this thesis, we studied the enhancement of quantum entanglement induced by optical parametric amplifiers in a hybrid cavity magnomechanical system. The hybrid configuration we investigated involves magnons, cavity microwave photons, and phonons. We constructed the model and Hamiltonian to describe our system. The system's dynamics were determined using the nonlinear quantum Langevin equations and the linearization approximation. In this framework, the bipartite entanglements were evaluated through logarithmic negativity. It turned out that the bipartite entanglements were enhanced when an optical parametric amplifier was present. In the same way, OPA improved entanglement's resistance to temperature. The relaxation of the prerequisite for strong magnon-phonon coupling, which was required in the absence of OPA to produce cavity-magnon entanglement, was another important effect of the OPA. Furthermore, in comparison to the system in which the optical parametric amplifier (OPA) was absent, the inclusion of the OPA not only strengthened the entanglement but also expanded its domain over a larger range of detunings. We believe that the technique that was given is a step towards realizing robust quantum entanglement with the available technology.

Contents

1

Introduction

1.1 Background of the Study

The field of quantum optics has seen significant growth in the last two decades, with a focus on quantum mechanical effects (Zhang et al., 2016b). This growth is expected to continue, with potential applications in computation, communication, and metrology (Cirac and Kimble, 2017). Quantum optics has also been instrumental in the development of photonic quantum simulators, which have the potential to address outstanding problems in physics, chemistry, and biology (Cao et al., 2019). Moreover, the field has been instrumental in the development of quantum computing and quantum key distribution, among other quantum technologies.

Quantum magnomechanics, a burgeoning field at the intersection of quantum optics and magnonics, has recently attracted interest due to its promising applications in quantum information processing and sensing(Zhou et al., 2023). This field is part of the broader area of quantum optomechanics, which investigates how light and mechanical devices interact quantum mechanically (Brawley et al., 2016). The potential applications of quantum magnomechanics have been further enlarged by the creation of hybrid quantum systems based on magnonics that can interact with optical photons, phonons, and superconducting qubits (Lachance-Quirion et al., 2019). These advancements highlight the growing importance of quantum magnomechanics in the field of quantum optics.

A study in the field of quantum magnomechanics has made significant strides in understanding and manipulating quantum phenomena. (Gorbatsevich et al., 1994)explored magnetoelectric phenomena in nanoelectronics, which could have implications for quantum magnomechanics. (Lachance-Quirion et al., 2019) demonstrated the ability to resolve a millimeter-sized ferromagnet, quanta of collective spin excitation, a key development in the field. These studies collectively highlight the potential for further advancements in quantum magnomechanics.

Recent research in the field of quantum magnomechanics has revealed the potential for creating squeezed states of magnons and phonons(Asjad et al., 2023). This is a significant development, as it opens up new possibilities for exploring the unique quantum properties of magnons(Kamra et al., 2020). Furthermore, the Bose-Einstein condensation of magnons in quantum magnets has been shown to lead to the emergence of ferroelectricity, a phenomenon with potential applications in multi-functional quantum magnets (Kimura et al., 2016). The integration of magnons with other quantum systems, such as microwave photons and acoustic phonons, has also been identified as a promising avenue for quantum engineering (Awschalom et al., 2021).

Also studies have explored the generation and enhancement of quantum entanglement in quantum magnomechanical systems. (Zuo et al., 2024) describes the creation of entangled states in cavity magnomechanical systems. (Wang, 2022) shows the generation of tripartite entanglement in a cavity magnomechanical system. These studies collectively highlight the potential for quantum entanglement in quantum magnomechanics and its applications in quantum state engineering and quantum information processing.

The most state of light which enhances entanglement in an optomechanics system is the squeezed state of light (Amazioug et al., 2020). This state, characterized by reduced quantum noise in one of its quadratures, has been shown to significantly enhance entanglement and quantum correlations in various optomechanical systems. For instance,(Amazioug et al., 2020)demonstrated that broadband squeezed light can enhance entanglement between mechanical modes in Fabry–Pérot cavities, while (Kalita et al., 2022) achieved enhanced entanglement between optical and LC circuit modes in an optoelectromechanical system. (Liao et al., 2018) further showed that steady-state bosonic squeezing and entanglement can be significantly enhanced in a dissipative optomechanical system through amplitude modulation.

The use of a degenerate parametric oscillator as a source of squeezed light is a key focus in the literature. (Pérez-Arjona et al., 2004)further explores this, showing that any optical dissipative structure supported by such oscillators contains a special transverse mode free from quantum fluctuations.(Marty et al., 2021) builds on this work, reporting on a new class of optical parametric oscillators based on a semiconductor photonic crystal cavity, which operates at telecom wavelengths and behaves as an ideal degenerate optical parametric oscillator. These studies collectively highlight the potential of degenerate parametric oscillators as a reliable source of squeezed light. In this thesis we consider a role of degenerate parametric oscillator in a cavity magnomechanical system.

1.2 Statement of the problem

Nowadays, there is great advancement in field of magnomechanical system, especially in understanding the interaction between magnons, phonons and photons but still many critical challenges remain unaddressed. The particular challenge is the enhancement of entanglement in these systems. Existing study focus on strong magnon-phonon coupling which is great barrier to maintain it in experimental setup. This strong magnon-phonon requirement limit cavity magnomechanical system to use it in quantum technologies (Jaeger, 2007).

Moreover, another major challenge is the external influence like thermal fluctuation remain significant concern. Quantum systems are inherently sensitive to external perturbations, thus, the resilience of quantum entanglement against these factors is crucial for its use in real-world applications(Sadiek and Kais, 2013).

Significant enhancements in bipartite entanglement between two optical modes and a mechanical mode have been achieved by incorporating an optical parametric amplifier. This device produces a squeezed light, effectively boosting the entanglement. Therefore, in this thesis the bipartite entanglement dynamics in cavity magnomechanical assisted by Optical Parametric Amplifier will be studied. We seek to understand how the presence of an Optical Parametric Amplifier (OPA) in this system leads to stabilization and enhancement of the entanglement.

1.3 Objective of the study

1.3.1 General Objective

The general objective of this thesis is to enhance the bipartite entanglement in a cavity magnomechanical system by optical parametric amplifier.

1.3.2 Specific Objective

- To obtain the Quantum Langevin equations in a hybrid magnomechanical system under the proposed model.
- To quantify the enhancement of bipartite entanglement between subsystems in the cavity magnomechanical model with the inclusion of an optical parametric amplifier.
- To identify and analyze the dynamical parameters of magnons, photons, and phonons within our hybrid cavity magnomechanical system.

1.4 Significance of the study

The significance of our study lies in presenting a method to enhance quantum entanglement within a cavity magnomechanical system. Enhancing entanglement is vital for the advancement of quantum computing and quantum communication, as entanglement is fundamental to quantum technology devices. Our research aligns with ongoing efforts to address limitations in quantum information processing by utilizing an optical parametric amplifier in the cavity magnomechanical system. This effort represents a significant step toward realizing advanced quantum technologies and expanding the capabilities of quantum information processing.

2

Literature Review

In this chapter we will see the basics of cavity magnomechanical system. We will also look at Zeeman interaction, magnomechanical interaction, optical parametric amplifier. Furthermore we will discuss the Quantum Langevin Equations and the linearization approach. Finally we will touch upon the logarithmic negativity concepts.

2.1 Cavity magnomechanics

Traditional forces such as radiation, electrostatic, and piezoelectric have facilitated the coupling of phonons with optical or microwave photons, spurring the development of cavity electro and optomechanical systems(Teufel et al., 2011). Despite their advancements, these systems are limited by their tunability. In contrast, the magnetostrictive force emerges as a viable alternative, enabling the coupling of magnons a tunable collective excitation of magnetization with phonons (Zahn, 2006). This interaction, previously overlooked due to its minimal presence in dielectric or metallic materials, is robust in magnetic materials, paving the way for highly tunable hybrid systems in coherent information processing.

Among magnetic materials, yttrium iron garnet (YIG) is unique because of its exceptional qualities. Renowned for its minimal loss for various information carriers such as magnons, acoustic phonons and microwave photons and its transparency to infrared light, YIG is an ideal candidate for integrating magnonic systems with optomechanical elements as illustrated in Figure 2.1.

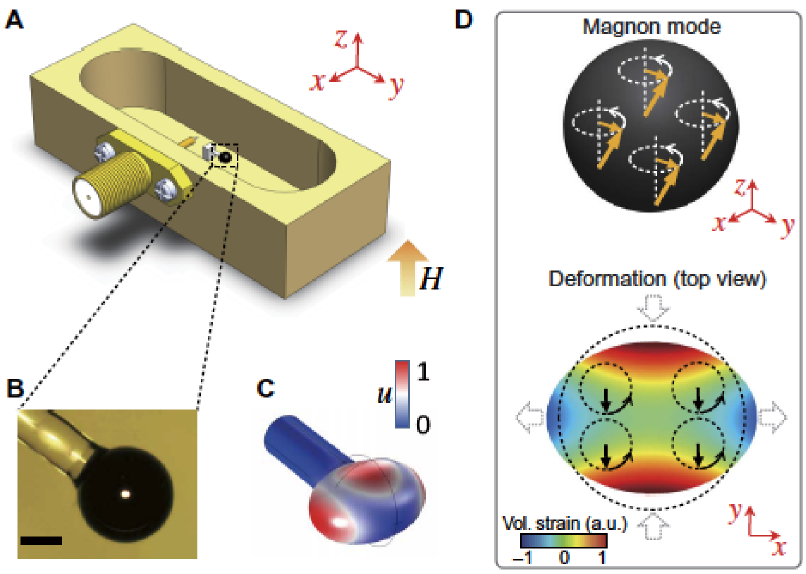

Figure 2.1: Device schematic of a typical Cavity magnomechanical system. (A) Schematic of a cavity containing a YIG sphere in three dimensions. (B) Optical picture of the YIG sphere with a diameter of 250 μm, polished to perfection.(C) The $S_{1,2}$ phonon mode's of mechanical displacement. (D) strain-induced Dynamic magnetization fields and uniform magnon excitation in the YIG sphere.(Zhang et al., 2016b)

.

Because of its integration capability, YIG is a great platform for transferring quantum states between various physical systems, which improves the performance of magnonic technologies (Zhang et al., 2014).

2.1.1 Hybrid Magnonic System

An essential part of the continuous advancement of quantum and classical technologies is hybrid systems. By combining two or more degrees of freedom, these systems try to take advantage of each subsystem's advantages while avoiding its disadvantages (Xiang et al., 2013). Spin ensembles coupled to superconducting qubits, for instance, might enable quantum memory, or mechanical oscillators coupled to optical and microwave photons at the same time could enable wavelength conversion (Julsgaard et al., 2013). As opposed to isolated subcomponents, the creation of hybrid systems ultimately yields a net gain in performance or extra capability. It has been demonstrated that the growth of many hybrid systems relies heavily on collective magnetic excitations, or magnons (Lachance-Quirion et al., 2017).

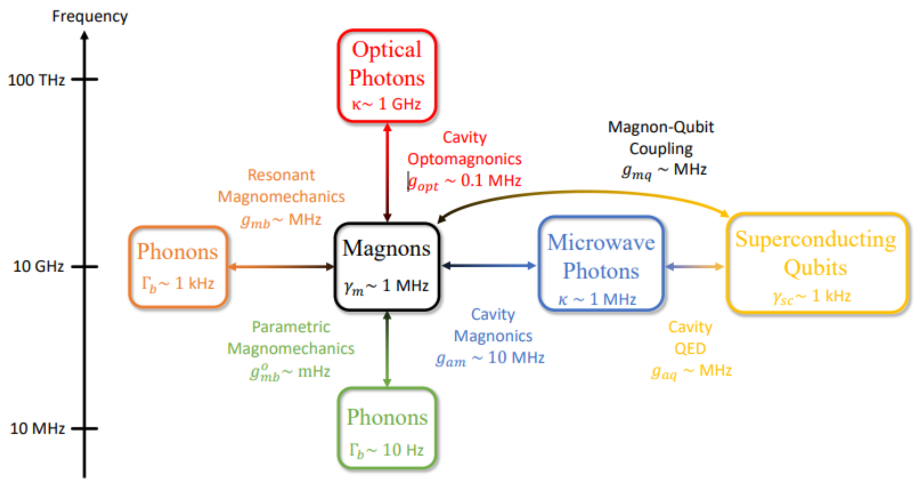

Figure 2.2: Characteristic frequency and the state-of-the-art decay rate and coupling rate for each hybrid magnonic system (Chumak et al., 2022).

As shown in Fgure 2.2, magnons play a central role in the development of many hybrid technologies . Magnons are versatile because they can couple to a large number of different supplementary subsystems. For instance, magnons housed in YIG pair parametrically with optical photons via magneto-optical effects and resonantly with microwave photons via the Zeeman interaction (Kusminskiy et al., 2016) .

Indirect coherent coupling between superconducting qubits and magnons has been made possible by microwave magnon coupling(Tabuchi et al., 2015). The measurement of the magnon number and single-shot magnon detection have all been made possible via microwave magnon coupling. A direct coupling between magnons and superconducting qubits without the need for a microwave cavity intermediate has even been proposed in recent work (Kounalakis et al., 2022). In addition, a great deal of theoretical and practical research has been done on cavity optomagnonics, including studies on Brillouin light scattering, magnon heralding and novel optomagnonic cavity designs(Osada et al., 2018). The magnetoelastic effect further explains how magnons can be related to mechanical strain inside a magnetic sample (Kittel, 1949). The magnetic anisotropy found in many magnetic crystals is intimately associated with magnetoelastic coupling (Kittel, 1958).

2.2 Magnon-Photon Interaction

The Zeeman interaction, in which the time oscillating microwave field tries to align the time oscillating magnetic moments inside the ferromagnetic sample, is what causes the coupling between magnon and photon .The form of the interaction Hamiltonian is

$$H_{\text{int}} = -\mu_0 \int_{V_m} dV \mathbf{M} \cdot \mathbf{H}_c. \tag{2.1}$$

Here, M is the net magnetization of the ferromagnetic sphere, H_c is the magnetic field of microwave resonator, and μ_0 represents the magnetic permeability of free space, a fundamental constant that quantifies the ability of vacuum to transmit magnetic fields. The integral is taken over V_m, the volume over which the calculation is performed, with dV representing the differential volume element used in the integral (Flower et al., 2019).

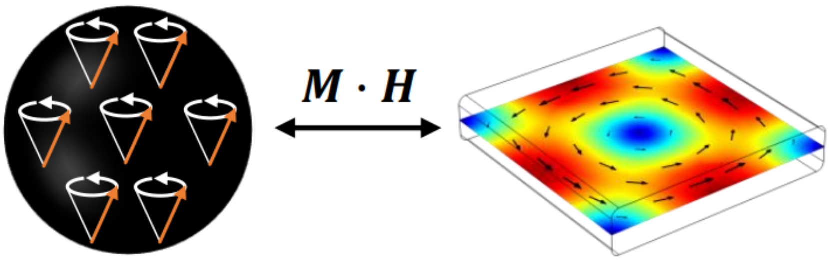

Figure 2.3: Schematic of magnon-photon coupling. Spins within the YIG sphere couple via the Zeeman interaction to the time-varying microwave cavity magnetic feld (Zhang et al., 2016b).

.

The quantized magnetic field mode of an empty microwave resonator can be expressed as follows after using this standard quantization protocol (Loudon, 2000).

$$H(r,t) = \frac{1}{\sqrt{\mu_0}} \sqrt{\frac{\mu_0 \hbar \omega_c}{2V_c}} h(r)(\hat{c} + \hat{c}^\dagger) \tag{2.2}$$

where h(r) is the normalized magnetic feld mode profle, $\hat{c}$ and $\hat{c}^\dagger$ are the annihilation and creation operators, respectively. ω_c represents the frequency at which the electromagnetic field oscillates.

Next, by defining a macrospin operator $S = \frac{V_m M}{\gamma}$, the uniform Kittel mode may be quantized. We have assumed that the magnetic sample has been saturated by a bias field in the z-direction, aligning the spins.The magnetization can be rewritten in terms of the raising and lowering spin operators $S^{\pm} = S_x \pm iS_y$ as,

$$M = \frac{\gamma}{V_m}\left(\frac{1}{2}(S^+ + S^-)\hat{x} + \frac{i}{2}(S^+ - S^-)\hat{y} + S_z\right). \tag{2.3}$$

Furthermore, the Holstein-Primakoff approximation can be used for low magnon numbers $\langle \hat{m}^\dagger \hat{m} \rangle \ll 2s$ to estimate the spin operators.

$$S^+ = \hbar\sqrt{2s}\hat{m}, \tag{2.4}$$

$$S^- = \hbar\sqrt{2s}\hat{m}^\dagger, \tag{2.5}$$

$$S_z = \hbar(s - \hat{m}^\dagger \hat{m}), \tag{2.6}$$

where the magnon formation and annihilation operators are denoted by $\hat{m}^\dagger$ and $\hat{m}$, respectively, and s is the total number of spins. By inserting these definitions to Equation 2.3, we are able to write

$$M = \frac{\gamma\hbar}{V_m}\left(\frac{\sqrt{2s}}{2}(\hat{m} + \hat{m}^\dagger)\hat{x} + \frac{i\sqrt{2s}}{2}(\hat{m} - \hat{m}^\dagger)\hat{y} + (s - \hat{m}^\dagger\hat{m})\hat{z}\right). \tag{2.7}$$

We can assume, without losing generality, that h(r) = $h(r)\hat{x}$ if we take into account the experimentally important scenario when the microwave cavity magnetic field overlying the magnetic sample is spatially uniform through the magnetic sample. The interaction Hamiltonian Eqn. 2.1 is obtained by inserting the magnetic field defined in Eqn. 2.2 and the net magnetization defined in Eqn 2.7.

$$\hat{H}_{\text{int}} = -\mu_0 \int_{V_m} dV \left(\frac{1}{\mu_0}\sqrt{\frac{\mu_0\hbar\omega_c}{2V_c}}h(r)(\hat{c} + \hat{c}^\dagger)\right)\frac{\gamma\hbar\sqrt{2s}}{2V_m}(\hat{m} + \hat{m}^\dagger). \tag{2.8}$$

By using the rotating wave approximation, we may simplify this further by assuming that the magnon-photon detuning is minimal $(\Delta_{ma} \ll \{\omega_a, \omega_m\})$. Then the Hamiltonian of interaction can be expressed as

$$\hat{H}_{\text{int}} = -\frac{\hbar\gamma}{2}\sqrt{\frac{\mu_0 s\hbar\omega_c}{V_c}}(\hat{c}\hat{m}^\dagger + \hat{c}^\dagger\hat{m})\int_{V_m} dV \frac{h(r)}{V_m}. \tag{2.9}$$

We may extract the magnetic field from the integral if we assume that the magnetic sample is tiny in relation to the length over which the magnetic field varies, so that h(r) is uniform over the whole volume V_m. Generally speaking, this integral could be explicitly performed as detailed in (Flower et al., 2019). However, in the majority of experimental scenarios, this approximation maintains a high degree of accuracy. Given the normalization of the magnetic field, we can define the mode overlap as

$$\eta = \frac{|h(r_m)|}{\max(|h(r)|)}$$

where η denotes the magnetic sample and cavity magnetic field overlap and r_m represents the magnetic sample's location Zhang et al. (2016b) . The interaction Hamiltonian can now be expressed as

$$\hat{H}_{int} = -\frac{\hbar\gamma\eta}{2}\sqrt{\frac{\mu_0 s\hbar\omega_c}{V_a}}(\hat{c}\hat{m}^\dagger + \hat{c}^\dagger\hat{m}) \tag{2.10}$$

alternatively, as we will use throughout the remainder of this thesis, we can write

$$\hat{H}_{\text{int}} = \hbar g_{cm}(\hat{c}m^\dagger + \hat{c}^\dagger\hat{m}) \tag{2.11}$$

where

$$g_{cm} = -\frac{\gamma}{2}\eta\sqrt{\frac{\mu_0 s\hbar\omega_c}{V_c}}, \tag{2.12}$$

is the coupling rate between magnons and photons is influenced by both the profile of the microwave cavity mode and the dimensions of the magnetic sample. Then total Hamiltonian describing the magnon-photon system which is given by

$$H = \hbar\omega_c\hat{c}^\dagger\hat{c} + \hbar\omega_m\hat{m}^\dagger\hat{m} + \hbar g_{cm}(\hat{c}\hat{m}^\dagger + \hat{c}^\dagger\hat{m}) \tag{2.13}$$

The Hamiltonian H consists of three primary terms. The first term, $\hbar\omega_c\hat{c}^\dagger\hat{c}$, represents the energy of the photon field, where $\hbar$ is the reduced Planck constant, ω_c is the angular frequency of the photon mode, and $\hat{c}^\dagger\hat{c}$ is the photon number operator that counts the number of photons in the mode. The second term, $\hbar\omega_m\hat{m}^\dagger\hat{m}$, describes the energy of the magnon field, with ω_m as the angular frequency of the magnon mode and $\hat{m}^\dagger\hat{m}$ as the magnon number operator. The third term, $\hbar g_{cm}(\hat{c}^\dagger\hat{m} + \hat{c}\hat{m}^\dagger)$, reflects the interaction between the photon and magnon fields, mediated by the coupling constant g_{cm}. This interaction term includes processes where energy is exchanged between photons and magnons, leading to the creation or annihilation of quanta in each field.

2.3 Magnon-Phonon interaction

The energy of the orbital state will depend on the orientation with respect to Spin-orbit coupling, which will cause the energy of the net magnetic moment to depend on their orientation within the crystal lattice if ions within the crystal lattice distort the electronic orbitals within the crystal. This orientation-dependent energy is called the magnetocrystalline anisotropy energy (Darby and Isaac, 1974). The following symmetry requirements must be satisfied by the anisotropy energy due to the cubic symmetry of the underlying crystal structure of YIG (Stancil and Prabhakar, 2009). First, the anisotropy energy must be invariant when the net magnetization M reverses . Second, the anisotropy energy must not vary when any two axes are switched. It is observable that the function that satisfies these conditions is

$$E_K = K_1(\alpha_1^2\alpha_2^2 + \alpha_2^2\alpha_3^2 + \alpha_3^2\alpha_1^2) + K_2\alpha_1^2\alpha_2^2\alpha_3^2 \tag{2.14}$$

Here, E_K represents the anisotropy energy, K_1 and K_2 are constants that quantify the energy contributions from specific orientations, and α_1, α_2, and α_3 are the directional cosines that relate the magnetization direction to the Cartesian axes. This framework determines the preferred magnetization directions that minimize the energy, reflecting the material's crystallographic structure and inherent properties. Taylor expansion may be used to represent the anisotropy energy's strain dependency (Lee, 1955).

$$E_K = E_K^0 + \frac{\partial E_K}{\partial \varepsilon_{ij}}\varepsilon_{ij} + \dots \tag{2.15}$$

The magnetoelastic energy E_M is given by

$$E_M = \frac{\partial E_k}{\partial \varepsilon_{ij}}\varepsilon_{ij} = b_{ijk}\varepsilon_{ij},$$

which, due to the crystal symmetry, can be reduced to two terms with coefficients,

$$\frac{\partial E_k}{\partial \varepsilon_{ii}} = b_1\alpha_i^2, \quad \frac{\partial E_k}{\partial \varepsilon_{ij}} = 2b_2\alpha_i\alpha_j.$$

Where b_1 and b_2 are known as the Kittel magnetoelastic coupling constants.

$$E_M = b_1\left(\alpha_x^2\varepsilon_{xx} + \alpha_y^2\varepsilon_{yy} + \alpha_z^2\varepsilon_{zz}\right) + 2b_2\left(\alpha_x\alpha_y\varepsilon_{xy} + \alpha_y\alpha_z\varepsilon_{yz} + \alpha_z\alpha_x\varepsilon_{zx}\right) \tag{2.16}$$

The relationship between the magnetization and Cartesian coordinates is

$$\alpha_i = \frac{M_i}{M_s} \tag{2.17}$$

Using these definitions, the magnetoelastic energy, in Cartesian coordinates, takes the form Zhang et al. (2016b).

$$E_M = \frac{b_1}{M_s^2}\left(M_x^2\varepsilon_{xx} + M_y^2\varepsilon_{yy} + M_z^2\varepsilon_{zz}\right) + \frac{2b_2}{M_s^2}\left(M_xM_y\varepsilon_{xy} + M_yM_z\varepsilon_{yz} + M_zM_x\varepsilon_{zx}\right) \tag{2.18}$$

The spin operators can be used to represent the magnetization as

$$M_x = \frac{\gamma\hbar\sqrt{2S}}{V_m}\frac{1}{2}(\hat{m} + \hat{m}^\dagger) \tag{2.19}$$

$$M_y = \frac{\gamma i\hbar\sqrt{2S}}{V_m}\frac{1}{2}(\hat{m} - \hat{m}^\dagger) \tag{2.20}$$

$$M_z^2 = M_s^2 - M_x^2 - M_y^2 \tag{2.21}$$

Here, we've assumed that there is a powerful external magnetic field that will align every spin in the direction of $\hat{z}$. As a result,

$$M_z \approx M_s - \frac{\hbar\gamma}{V_m}\hat{m}^\dagger\hat{m} \tag{2.22}$$

Quantized displacement of a mechanical oscillator is defined as (Hauer et al., 2013)

$$\hat{u}(r,t) = \hat{x}(t)u(r), \tag{2.23}$$

where $\hat{x}(t) = x_{zpf}[\hat{b} + \hat{b}^\dagger]$ and $x_{zpf} = \sqrt{\frac{\hbar}{2m_{\text{eff}}\Omega_b}}$. Moreover, we defined $u(r)$ as the normalized displacement profile such that $\max|u(r)| = 1$. Given this definition, we can write the strain induced by a single phonon as

$$\varepsilon_{ij} = x_{zpf}\left(\hat{b} + \hat{b}^\dagger\right)\frac{1}{2}\left(\frac{\partial u_i}{\partial x_j} + \frac{\partial u_j}{\partial x_i}\right) \tag{2.24}$$

When resonant, the second term in Eq.(2.18) can lead to either linear magnon-phonon coupling or parametric magnon creation if the phonon frequency is double the magnon frequency. We will just be concentrating on the first Hamiltonian for this work. when these quantized operators are substituted in to the first term of the magnetoelastic energy in Eq. (2.18) it becomes.

$$H_1 = \frac{b_1}{M_s^2}\int_V dV\left(M_x^2\varepsilon_{xx} + M_y^2\varepsilon_{yy} - (M_x^2 + M_y^2)\varepsilon_{zz}\right) \tag{2.25}$$

$$= \frac{\hbar\gamma b_1}{M_s}\hat{m}^\dagger\hat{m}\left(\hat{b} + \hat{b}^\dagger\right)\frac{x_{zpf}}{V_m}\int_V dV\left(\varepsilon_{xx} + \varepsilon_{yy} - 2\varepsilon_{zz}\right) \tag{2.26}$$

This term is equivalent to the optomechanical coupling Hamiltonian and represents a parametric coupling between magnons and phonons and can be written as follows.

$$H = \hbar g_{mb} \hat{m}^{\dagger} \hat{m} \left(\hat{b} + \hat{b}^{\dagger} \right) \tag{2.27}$$

where

$$g_{mb}^{0} = \frac{1}{\hbar} b_1 \zeta \tag{2.28}$$

is the single magnon-phonon coupling rate. Recall $n_s = 2.2 \times 10^{28}\ \mathrm{m}^{-3}$ is the spin density of YIG and ζ is defined as

$$\zeta = \frac{x_{zpf}}{V_m} \int_V dV (\varepsilon_{xx} + \varepsilon_{yy} - 2\varepsilon_{zz}) \tag{2.29}$$

It is the single phonon strain overlap integral.

2.4 Optical Parametric Amplifiers

The optical parametric amplifier, a key device in the field of quantum optics, has garnered significant interest due to its well-characterized properties(Cerullo and De Silvestri, 2003). The significance of OPA extends beyond mere amplification. It plays a crucial role in generating squeezed state of light, which is fundamental for quantum information processing, quantum metrology, and various other applications in quantum technologies. Squeezed states of light reduce quantum noise in one field quadrature at the expense of increased noise in the orthogonal quadrature, allowing for measurements that can surpass the standard quantum limit. This characteristic is exceptionally beneficial for improving the precision of measurements, such as those required in gravitational wave detection, where reducing quantum noise can significantly enhance the signal-to-noise ratio.

This process is fundamental to the exploration and manipulation of quantum states in optical systems. The optical parametric amplifier stands as a pivotal and extensively studied device in quantum optics. In these amplifiers, a high-energy pump photon undergoes an interaction within a cavity, mediated by a nonlinear crystal. This process results in the pump photon being down-converted into two photons, each possessing a lower frequency. Such mechanisms are integral to advancing our understanding and control of quantum states in optical frameworks(Zhang et al., 2016a)(Abebe et al., 2020).

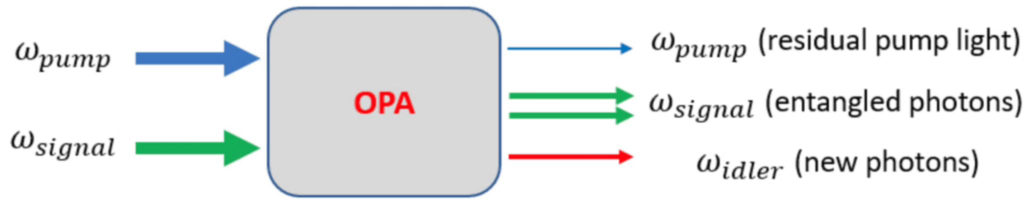

Figure 2.4: Degenerate optical parametric amplifier with a nonlinear crystal that is driven by coherent light(Baumgartner and Byer, 1979).

2.5 Tools of quantum magnomechanical systems

In quantum magnomechanical systems, several advanced techniques and concepts are crucial for understanding the dynamics and interactions at the quantum level. These include the quantum Langevin equations, the linearization approximation approach, and the logarithmic negativity method.

2.5.1 The quantum Langevin equations

In quantum mechanics, particularly within the Heisenberg picture, the time evolution of a system is uniquely defined by the evolution of its operators rather than its state vectors. This perspective is instrumental in understanding the dynamics of quantum systems, especially when extended to more complex scenarios like open quantum systems. The Heisenberg-Langevin equation serves as a pivotal extension of the standard Heisenberg equation of motion, incorporating the intricacies of open systems which are often characterized by dissipative and noisy environments.

In scenarios where the system exhibits dissipative behaviors, the Heisenberg equations of motion, commonly referred to as the quantum Langevin equations, are employed. These equations elegantly blend the deterministic evolution of operators with stochastic elements, representing the random influences of the surrounding environment. Formally, the equation is given as(Vitali et al., 2007)(Danaci, 2020)

$$\dot{\hat{Z}} = -\frac{i}{\hbar}[\hat{Z}, \hat{H}_T] + N - \gamma \hat{Z}, \tag{2.30}$$

where $\hat{Z}$ symbolizes any general operator variable such as $\hat{q}$, $\hat{p}$, or $\hat{a}$. The term γ stands for the damping coefficient, indicative of the dissipative nature of the system, while N represents the quantum noise, also known as Brownian noise, which averages to zero. This integration of deterministic and stochastic elements in the equation provides a comprehensive framework for analyzing the temporal behavior of quantum systems in realistic, non-isolated scenarios.

2.5.2 Linearization approximation approach

In the context of magnomechanical systems, the linearized approximation provides an insightful method for grasping the dynamics of such coupled systems. This approach is particularly useful as it allows the exact solution of linear dynamics in principle. The linearized Langevin equations for magnomechanics are derived using a similar approximation as in cavity optomechanics. Here, the dynamics involve a Heisenberg operator that comprises a steady-state value plus a fluctuating operator with a zero mean value(Vashahri-Ghamsari et al., 2021). This adjustment is achieved by increasing the drive power, and with sufficiently strong drive, the system's dynamics are essentially quantum fluctuations around a classical steady state. The operator for a magnomechanical system, analogous to the optical field amplitude in optomechanics, can be expressed as

$$\hat{a} = \alpha + \delta\hat{a}, \tag{2.31}$$

where α represents the mean field amplitude of the system, and $\delta\hat{a}$ denotes the fluctuations. When expanding it's possible to neglect terms like α^2 as it leads to a constant force that merely shifts the system's equilibrium position. The driving term from the standard Hamiltonian is excluded from the linearized Hamiltonian, as it is the origin of the classical amplitude α around which the linearization is performed.

2.5.3 Logarithmic negativity approach

Logarithmic negativity is a widely recognized tool for measuring the degree of entanglement between two systems, regardless of their size. It is extensively used by researchers to compute the entanglement of mixed states, explore its spatial distribution, capture quantum correlations, and quantify continuous-variable Gaussian-type bipartite states. Its popularity stems from its explicit computability and additive properties.The generated continuous-variable (CV) bipartite entanglement is measured in terms of logarithmic negativity E_N, defined as Dias (2020).

$$E_N = \max[0, -\ln 2\eta_-], \tag{2.32}$$

where η_- is the minimum symplectic eigenvalue of the partially transposed cavity mode corresponds to the interest bipartite system. It is given by

$$\eta_- = \frac{1}{\sqrt{2}}\sqrt{\Sigma(V) - \sqrt{\Sigma(V)^2 - 4\det V}}, \tag{2.33}$$

where V is the covariance matrix, expressed as a block matrix

$$V = \begin{pmatrix} B & C \\ C^T & B' \end{pmatrix}, \tag{2.34}$$

and $\Sigma(V) = \det B + \det B' - 2\det C$. Here, B, C, and B' are 2×2 matrices derived from the correlation matrix. E_N indicates entanglement if $\det C < 0$ and $\eta_- \leq \frac{1}{2}$. Utilizing this framework, the bipartite entanglement between two modes can be measured (Javanmard et al., 2018)(Ruggiero et al., 2016).

3

Methodology

3.1 Overview

In this chapter we focus on the comprehensive modeling and analysis of cavity magnomechanical systems enhanced by an Optical Parametric Amplifier (OPA). This includes a detailed exploration of the Model and Hamiltonian of the System, which lays the foundational theoretical framework; dynamics of the system, where the behavior under dynamic conditions is examined through nonlinear quantum Langevin equations; the steady state equations motion of the system, which explores the system's behavior at equilibrium; and the fluctuation equations motion of the system, where small deviations from equilibrium are analyzed to understand the system's response to perturbations.

3.2 Model and Hamiltonian of the system

The model we are going to study is a cavity magnomechanical system that incorporates a ferrimagnetic crystal which is yttrium iron garnet in microwave cavity. This configuration is pivotal to study interaction among various quantum element in magnomechanical system. The YIG sphere which we use in this study is selected because of its high spin density and low energy dissipation rate. It serve as medium for magnon excitation. These are collective spins in the sphere and it interacts with electromagnetic field through magnetic dipole interaction. The system also accommodates phonons, which are collective mechanical excitations in the material.

A main feature of our model is the integration of optical parametric amplifier in

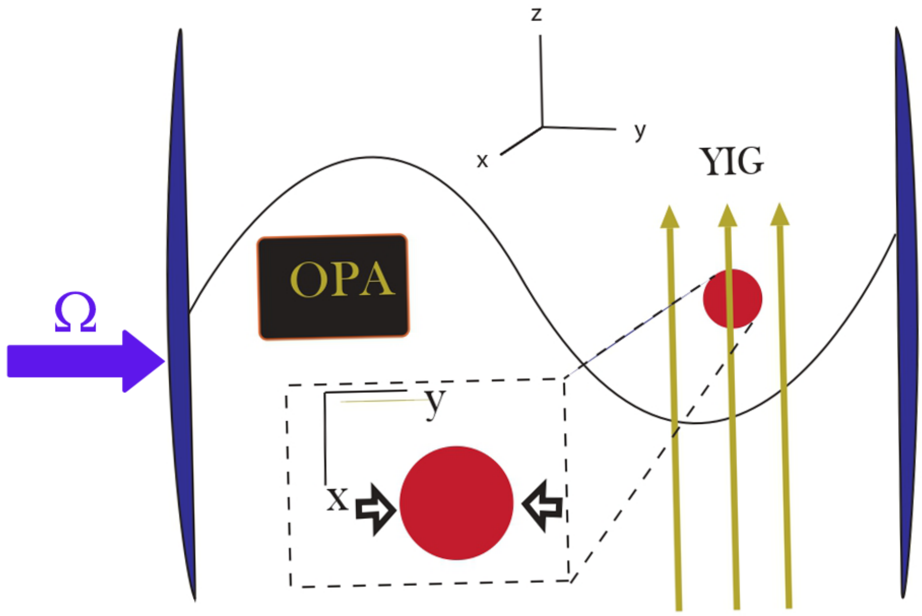

Figure 3.1: Schematic diagram of our model, which is magnomechanical system that consist an Optical Parametric Amplifier (OPA) and a YIG sphere in a microwave cavity .

cavity magnomechanical system. OPA has ability to amplify and attenuate photon signal (Lam et al., 1998). It also generate squeezed state of light wich is expected to influence the quantum dynamics of the system. The Hamiltonian of our system is given by

$$
\begin{aligned}
H = {} & \hbar\omega_c \hat{c}^\dagger \hat{c} + \hbar\omega_m \hat{m}^\dagger \hat{m} + \frac{\omega_b}{2}(q^2 + p^2) + \\
& \hbar g_{mb} \hat{m}^\dagger \hat{m} \left(\hat{b} + \hat{b}^\dagger\right) + \hbar g_{mc}(c^\dagger m + c m^\dagger) + \\
& i\hbar G \left(e^{i\theta} \hat{c}^{\dagger 2} e^{-i\omega t} - e^{-i\theta} \hat{c}^2 e^{i\omega t}\right) + i\hbar\Omega \left(\hat{m}^\dagger e^{-i\omega t} - \hat{m} e^{i\omega t}\right) \quad . \qquad (3.1)
\end{aligned}
$$

The Hamiltonian effectively encapsulates each terms representing specific physical interactions and properties. The initial terms, $\hbar\omega_c \hat{c}^\dagger \hat{c}$ and $\hbar\omega_m \hat{m}^\dagger \hat{m}$, correspond to the energies of the cavity and magnon modes, where $\hat{c}^\dagger$, $\hat{c}$, $\hat{m}^\dagger$, and $\hat{m}$ are the creation and annihilation operators for photons in the cavity and magnons, respectively. The third term, $\frac{\omega_b}{2}(q^2 + p^2)$, describes the energy of the mechanical (phonon) mode, with q and p being its position and momentum quadratures. The magnon-phonon interaction is indicated by the fourth term, $\hbar g_{mb} \hat{m}^\dagger \hat{m} \left(\hat{b} + \hat{b}^\dagger\right)$, where g_{mb} is the rate of magnomechanical coupling.

The coupling between magnons and the microwave cavity is articulated by the fifth term, $\hbar g_{mc}(c^\dagger m + c m^\dagger)$, with the rate g_{mc} indicating strong coupling if it surpasses the cavity (κ_c) and magnon (κ_m) mode dissipation rates. The OPA's nonlinear gain is depicted by the sixth term, $i\hbar G\left(e^{i\theta}\hat{c}^{\dagger 2}e^{-i\omega t} - e^{-i\theta}\hat{c}^2 e^{i\omega t}\right)$, where G and θ denote the gain and the driving field's phase. The strength of the microwave field driving the magnon mode, defined by the Rabi frequency $\Omega = \frac{\sqrt{5}}{4}\gamma\sqrt{NB_0}$, is described lastly, where γ represents the gyromagnetic ratio, and $N = \rho V$ indicates the overall spin count within the YIG sphere, considering its spin density ρ and volume V. Radiation pressure effects are disregarded based on the assumption that the microwave field's wavelength greatly exceeds the sphere's size.

3.3 Dynamics of the system

The Hamiltonian describing the system's energy and interactions is outlined in Equation (3.1). From this Hamiltonian, a series of nonlinear quantum Langevin equations can be formulated to model the dynamics of the Magnomechanical Systems equipped with an Optical Parametric Amplifier (OPA).
In equ 3.1 the fourth term describes magnon phonon intraction:

$$H_4 = \hbar g_{mb}\hat{m}^\dagger\hat{m}\left(\hat{b} + \hat{b}^\dagger\right) \tag{3.2}$$

Where the annihilation and creation operators of mechanical resonators are $\hat{b}$ and $\hat{b}^\dagger$, respectively, while the annihilation and creation operators of the magnon mode frequency are $\hat{m}$ and $\hat{m}^\dagger$. They are described as

$$\hat{b} = \frac{m\omega_m\hat{x} + i\hat{p}}{\sqrt{2m\omega_m\hbar}} \tag{3.3}$$

$$\hat{b}^\dagger = \frac{m\omega_m\hat{x} - i\hat{p}}{\sqrt{2m\omega_m\hbar}} \tag{3.4}$$

in which

$$\hat{x} = q\sqrt{\frac{\hbar}{m\omega_m}} \tag{3.5}$$

and

$$\hat{p} = p\sqrt{m\hbar\omega_m}. \tag{3.6}$$

Then the term $\hat{b}+\hat{b}^{\dagger}$ in Eq. (3.2) can be written as

$$\hat{b}+\hat{b}^{\dagger}=\left(\frac{m\omega_m\hat{x}}{\sqrt{2m\hbar\omega_m}}-\frac{i\hat{p}}{\sqrt{2m\hbar\omega_m}}\right)+\left(\frac{m\omega_m\hat{x}}{\sqrt{2m\hbar\omega_m}}+\frac{i\hat{p}}{\sqrt{2m\hbar\omega_m}}\right)=\frac{2m\omega_m\hat{x}}{\sqrt{2\hbar m\omega_m}}. \quad (3.7)$$

Now, after inserting Eq. (3.5) into Eq. (3.7) with $\frac{2}{\sqrt{2}}\approx 1$ we get

$$\hat{b}+\hat{b}^{\dagger}=q. \quad (3.10)$$

Finally, by inserting Eq.(3.10) in to Eq.(3.2) we get

$$H_4=\hbar g_{mb}\hat{m}^{\dagger}\hat{m}\hat{q} \quad (3.8)$$

The driving Hamiltonian $\hat{H}_d$ and parametric Hamiltonian $\hat{H}_p$ of our system are as follows:

$$\hat{H}_d=i\hbar\Omega\left(\hat{m}^{\dagger}e^{-i\omega t}-\hat{m}e^{i\omega t}\right), \quad (3.9)$$

$$\hat{H}_p=i\hbar G\left(e^{i\theta}\hat{c}^{\dagger 2}e^{-i\omega t}-e^{-i\theta}\hat{c}^2e^{i\omega t}\right), \quad (3.10)$$

This terms are time dependent. To avoid time dependence of this terms we apply unitary transformation (Axline, 2018).

$$\hat{H}_d=U\hat{H}_dU^{\dagger}+i\hbar\frac{dU}{dt}U^{\dagger}. \quad (3.11)$$

$$\hat{H}_d=U\left[i\hbar\Omega\left(\hat{m}^{\dagger}e^{-i\omega t}-\hat{m}e^{i\omega t}\right)\right]U^{\dagger}+i\hbar\frac{dU}{dt}U^{\dagger} \quad (3.12)$$

Using

$$\begin{aligned}\hat{m}_f&=\hat{m}_ie^{-i\omega t},\\ \hat{m}_f{}^{\dagger}&=\hat{m}_i{}^{\dagger}e^{i\omega t},\\ \hat{U}&=e^{-i\omega\hat{m}^{\dagger}\hat{m}t},\\ \hat{U}^{\dagger}&=e^{i\omega\hat{m}^{\dagger}\hat{m}t},\\ \hat{U}\hat{U}^{\dagger}&=1\end{aligned}$$

We can express the driving Hamiltonian $\hat{H}_d$ as

$$\hat{H}_d=i\hbar\Omega(\hat{m}^{\dagger}-\hat{m})-\hbar\omega\hat{m}^{\dagger}\hat{m} \quad (3.13)$$

To overcome the time-dependence of Eq. (3.10), we have similarly applied a unitary transformation as

$$\tilde{H}_p = U\hat{H}_p U^\dagger + i\hbar\frac{dU}{dt}U^\dagger. \tag{3.14}$$

It then follows that

$$\tilde{H}_p = \tilde{U}\left[i\hbar G\left(e^{i\theta}\hat{c}^2 e^{-i\omega t} - e^{-i\theta}(\hat{c}^\dagger)^2 e^{i\omega t}\right)\right]\tilde{U}^\dagger + i\hbar\frac{dU}{dt}U^\dagger \tag{3.15}$$

so that using the relations

$$\begin{aligned}
\hat{c_f}^2 &= \hat{c_i}^2 e^{-i\omega t}\\
\hat{c_f}^{\dagger 2} &= \hat{c_i}^{\dagger 2} e^{i\omega t}\\
\hat{U} &= \exp\left(i\omega(\hat{c}^\dagger\hat{c})^2 t\right)\\
\hat{U}^\dagger &= \exp\left(-i\omega(\hat{c}^\dagger\hat{c})^2 t\right)\\
\hat{U}\hat{U}^\dagger &= 1
\end{aligned}$$

$\hat{H}_P$ could be rewritten as

$$\hat{H}_p = i\hbar G\left(e^{i\theta}\hat{c}^2 - e^{-i\theta}\hat{c}^{\dagger 2}\right) - \hbar\omega(\hat{c}^\dagger\hat{c})^2. \tag{3.16}$$

In Eq. (3.16), the final term disappears, having no bearing on our conclusion, and the equation then becomes

$$\hat{H}_p = i\hbar G\left(e^{i\theta}\hat{c}^2 - e^{-i\theta}\hat{c}^{\dagger 2}\right). \tag{3.17}$$

Our system's Hamiltonian in a frame rotating at the driving field's frequency under rotating-wave approximation is as follows

$$\begin{aligned}
\frac{H}{\hbar} = \Delta c^\dagger c + \Delta m^\dagger m + \frac{\omega_b}{2}(q^2+p^2) +&\\
g_{mb}\hat{m}^\dagger\hat{m}\hat{q} + g_{mc}(c^\dagger m + cm^\dagger) +&\\
iG(e^{i\theta}c^{\dagger 2} - e^{-i\theta}c^2) + i\Omega(m^\dagger - m).&
\end{aligned} \tag{3.18}$$

Now It is possible to compute the nonlinear QLE for this system.

for $\dot{\hat{q}}$

$$\frac{d\hat{q}}{dt} = \dot{\hat{q}} = -\frac{i}{\hbar}[\hat{q},\hat{H}] + N - \gamma\hat{q} \tag{3.19}$$

with the use of Eq.(3.18), we see that

$$[\hat{q},\hat{H}] = [\hat{q},\Delta\hat{c}^{\dagger}\hat{c}+\Delta\hat{m}^{\dagger}\hat{m}+\frac{\omega_b}{2}(\hat{q}^2+\hat{p}^2)+ \\ \hbar g_{mb}\hat{m}^{\dagger}\hat{m}\hat{q}+g_{mc}(\hat{c}^{\dagger}\hat{m}+\hat{c}\hat{m}^{\dagger})+ \\ iG(e^{i\theta}\hat{c}^{\dagger 2}-e^{-i\theta}\hat{c}^2)+i\Omega(\hat{m}^{\dagger}-\hat{m})]. \tag{3.20}$$

Or

$$\begin{aligned}[\hat{q},\hat{H}] =&[\hat{q},\Delta\hat{c}^{\dagger}\hat{c}]+[\hat{q},\Delta\hat{m}^{\dagger}\hat{m}]+[\hat{q},\frac{\omega_b}{2}(\hat{q}^2+\hat{p}^2)] \\ &+[\hat{q},\hbar g_{mb}\hat{m}^{\dagger}\hat{m}\hat{q}]+[\hat{q},g_{mc}(\hat{c}^{\dagger}\hat{m}+\hat{c}\hat{m}^{\dagger})] \\ &+[\hat{q},iG(e^{i\theta}\hat{c}^{\dagger 2}-e^{-i\theta}\hat{c}^2)]+[\hat{q},i\Omega(\hat{m}^{\dagger}-\hat{m})]. \end{aligned} \tag{3.21}$$

Employing the commutation relations

$$[\hat{A},\hat{B}\hat{C}] = \hat{B}[\hat{A},\hat{C}]+[\hat{A},\hat{B}]\hat{C} \tag{3.22}$$

$$[\hat{A}\hat{B},\hat{C}] = \hat{A}[\hat{B},\hat{C}]+[\hat{A},\hat{C}]\hat{B} \tag{3.23}$$

$$[\hat{q},\hat{p}] = i\hbar \tag{3.24}$$

and

$$[\hat{q},\hat{c}] = [\hat{q},\hat{c}^{\dagger}] = [\hat{q},\hat{m}] = [\hat{q},\hat{m}^{\dagger}] = 0 \tag{3.25}$$

We can put Eq.(3.19) as

$$\dot{q} = \omega_b p, \tag{3.26}$$

Moreover, the time evolution for the operator $\hat{p}$ can be written as

$$\frac{d\hat{p}}{dt} = \dot{\hat{p}} = -\frac{i}{\hbar}[\hat{p},\hat{H}]+N-\gamma\hat{p} \tag{3.27}$$

Taking Eq.(3.18) in to account,we notice that

$$\begin{aligned}[\hat{p},\hat{H}] =&[\hat{p},\Delta\hat{c}^{\dagger}\hat{c}]+[\hat{p},\Delta\hat{m}^{\dagger}\hat{m}]+[\hat{p},\frac{\omega_b}{2}(\hat{q}^2+\hat{p}^2)] \\ &+[\hat{p},\hbar g_{mb}\hat{m}^{\dagger}\hat{m}\hat{q}]+[\hat{p},g_{mc}(\hat{c}^{\dagger}\hat{m}+\hat{c}\hat{m}^{\dagger})] \\ &+[\hat{p},iG(e^{i\theta}\hat{c}^{\dagger 2}-e^{-i\theta}\hat{c}^2)]+[\hat{p},i\Omega(\hat{m}^{\dagger}-\hat{m})]. \end{aligned} \tag{3.28}$$

Using the commutation relations

$$[\hat{p}, \hat{p}] = 0, \tag{3.29}$$

$$[\hat{p}, \hat{q}] = -i\hbar, \tag{3.30}$$

$$[\hat{p}, \hat{q}^2] = -i\hbar\hat{q}, \tag{3.31}$$

$$[\hat{p}, \hat{c}] = [\hat{p}, \hat{c}^\dagger] = 0, \tag{3.32}$$

$$[\hat{p}, \hat{m}] = [\hat{p}, \hat{m}^\dagger] = 0, \tag{3.33}$$

the time evolution in Eq.(3.27) can be expressed as:

$$\dot{\hat{p}} = -\omega_b\hat{q} - \gamma\hat{p} - g_{mb}\hat{m}^\dagger\hat{m} + \xi, \tag{3.34}$$

The time evolution of the microwave cavity mode operator can also be written as:

$$\frac{d\hat{c}}{dt} = \dot{\hat{c}} = -\frac{i}{\hbar}[\hat{c}, \hat{H}] + N - \gamma\hat{c} \tag{3.35}$$

Now with the aid of Eq.(3.18),we see that

$$\begin{aligned}[\hat{c}, \hat{H}] =& [\hat{c}, \Delta\hat{c}^\dagger\hat{c}] + [\hat{c}, \Delta\hat{m}^\dagger\hat{m}] + [\hat{c}, \frac{\omega_b}{2}(\hat{q}^2 + \hat{p}^2)] \\ &+ [\hat{c}, \hbar g_{mb}\hat{m}^\dagger\hat{m}\hat{q}] + [\hat{c}, g_{mc}(\hat{c}^\dagger\hat{m} + \hat{c}\hat{m}^\dagger)] \\ &+ [\hat{c}, iG(e^{i\theta}\hat{c}^{\dagger 2} - e^{-i\theta}\hat{c}^2)] + [\hat{c}, i\Omega(\hat{m}^\dagger - \hat{m})],\end{aligned} \tag{3.36}$$

Employing the commutation relations

$$[\hat{c}, \hat{q}] = 0$$

$$[\hat{c}, \hat{c}^\dagger] = 1$$

$$[\hat{c}, \hat{m}] = [\hat{c}, \hat{m}^\dagger] = 0$$

we can write Eq.(3.35) as

$$\dot{\hat{c}} = -(i\Delta_c + \kappa_c)\hat{c} - ig_{mc}\hat{m} + 2Ge^{i\phi}\hat{c}^\dagger + \sqrt{2\kappa_c}\hat{c}^{in} \tag{3.37}$$

In a similar manner, the time evolution for the magnon mode operator is expressible as:

$$\frac{d\hat{m}}{dt} = \dot{\hat{m}} = -\frac{i}{\hbar}[\hat{m}, \hat{H}] \tag{3.38}$$

and using the Hamiltonian described by Eq.(3.18), we see that

$$[\hat{m},\hat{H}] =[\hat{m},\Delta\hat{c}^{\dagger}\hat{c}]+[\hat{m},\Delta\hat{m}^{\dagger}\hat{m}]+[\hat{m},\frac{\omega_b}{2}(\hat{q}^2+\hat{p}^2)] \\ +[\hat{m},\hbar g_{mb}\hat{m}^{\dagger}\hat{m}\hat{q}]+[\hat{m},g_{mc}(\hat{c}^{\dagger}\hat{m}+\hat{c}\hat{m}^{\dagger})] \\ +[\hat{m},iG(e^{i\theta}\hat{c}^{\dagger 2}-e^{-i\theta}\hat{c}^2)]+[\hat{m},i\Omega(\hat{m}^{\dagger}-\hat{m})] \tag{3.39}$$

With the aid of the relations

$$[\hat{m},\hat{c}]=0, \tag{3.40}$$

$$[\hat{m},\hat{c}^{\dagger}]=0, \tag{3.41}$$

$$[\hat{m},\hat{m}^{\dagger}]=1, \tag{3.42}$$

$$[\hat{p},\hat{m}]=0, \tag{3.43}$$

$$[\hat{q},\hat{m}]=0, \tag{3.44}$$

we can put Eq.(3.38) as

$$\dot{\hat{m}}=-(i\Delta_m+\kappa_m)\hat{m}-ig_{mc}\hat{c}-ig_{mb}\hat{m}\hat{q}+\Omega+\sqrt{2\kappa_m}\hat{m}^{in}, \tag{3.45}$$

Thus, the system's quantum Langevin equations are provided by

$$\dot{\hat{c}}=-(i\Delta_c+\kappa_c)\hat{c}-ig_{mc}\hat{m}+2Ge^{i\theta}\hat{c}^{\dagger}+\sqrt{2\kappa_c}\hat{c}^{in}, \tag{3.46}$$

$$\dot{\hat{m}}=-(i\Delta_m+\kappa_m)\hat{m}-ig_{mc}\hat{c}-ig_{mb}\hat{m}\hat{q}+\Omega+\sqrt{2\kappa_m}\hat{m}^{in}, \tag{3.47}$$

$$\hat{q}=\omega_b\hat{p}, \tag{3.48}$$

$$\dot{\hat{p}}=-\omega_b\hat{q}-\gamma_b\hat{p}-g_{mb}\hat{m}^{\dagger}\hat{m}+\xi, \tag{3.49}$$

where the mechanical damping rate is represented by γ_b. The input noise operators for the cavity, magnon, and mechanical modes, respectively, are $\hat{c}^{in}$, $\hat{m}^{in}$, and $\hat{\xi}$. They have zero mean and are characterized by correlation functions as(Li et al., 2018).

$$\langle\hat{c}^{in}(t)\hat{c}^{in\dagger}(t')\rangle=[N_c(\omega_c)+1]\delta(t-t'), \tag{3.50}$$

$$\langle\hat{c}^{in\dagger}(t)\hat{c}_{in}(t')\rangle=N_c(\omega_c)\delta(t-t'), \tag{3.51}$$

$$\langle\hat{m}^{in}(t)\hat{m}^{in\dagger}(t')\rangle=[N_m(\omega_m)+1]\delta(t-t'), \tag{3.52}$$

$$\langle\hat{m}^{in\dagger}(t)\hat{m}^{in}(t')\rangle=N_m(\omega_m)\delta(t-t'), \tag{3.53}$$

$$\langle\hat{\xi}(t)\hat{\xi}(t')\rangle=\gamma_b[2N_b(\omega_b)+1]\delta(t-t'), \tag{3.54}$$

where a Markovian approximation has been performed, which is valid for a large mechanical quality factor $Q = \frac{\omega_b}{\gamma_b} \gg 1$, $\mathrm{N}_j(\omega_j) = \left[\exp\left(\frac{\hbar\omega_j}{k_B T}\right) - 1\right]^{-1}$ (j = c, m, b) are the equilibrium mean number of the thermal photon, magnon, and phonon, respectively.

3.4 The steady state equations of the system

If the magnon mode is substantially driven enough that $|\langle m\rangle| \gg 1$,The system's dynamics are linearizable.The cavity field amplitude $|\langle c\rangle| \gg 1$ is also substantial for a strong cavity-magnon interaction. Consequently, the operator $O = \langle O\rangle + \delta O$ ($O = c, m, q, p$) may be expressed in terms of both its steady-state value and a fluctuation portion up to first order. The steady-state mean value is represented by $\langle O\rangle$, while the small fluctuation operator δO has a zero mean value (Agasti, 2020).

$$c = c_s + \delta c, \tag{3.55}$$

$$m = m_s + \delta m, \tag{3.56}$$

$$q = q_s + \delta q, \tag{3.57}$$

$$p = p_s + \delta p, \tag{3.58}$$

where $\delta q, \delta p, \delta\alpha$ and δm are fluctuations with zero mean value and q_s, p_s, α_s, and m_s are the system's amplitude. The relevant average values are obtained by applying derivatives and setting the fluctuations to zero-mean values.

Using Eq.(3.58) in Eq.(3.48)

$$\delta\dot{q} = \omega_b(p_s + \delta p) \tag{3.59}$$

The momentum p_s has a mean value of zero in the steady-state, meaning that mechanical damping has no effect on the system's steady-state. Following that, $p_s = 0$

$$\delta\dot{q} = \omega_b \delta p$$

To find q_s, lets insert Eq. (3.56), Eq. (3.57) and Eq. (3.58) into Eq. (3.49)

$$\delta\dot{p} = -\omega_b(q_s + \delta q) - \gamma_b(p_s + \delta p) - g_{mb}(m_s^* + \delta m^*)(m_s + \delta m) + \xi(t) \tag{3.60}$$

Because of the steady-state momentum p_s equals zero and the fluctuation terms δq, δp, δm and δc have mean values of zero. we may write q_s as

$$q_s = -\frac{g_{mb}|m_s|^2}{\omega_m} \tag{3.61}$$

Then, Eq.(3.60) becomes

$$\delta\dot{p} = -g|m_s|^2 + g|m_s|^2 - \omega_m\dot{q} + g_{mb}(m_s\delta m_s^* + m_s{}^*\delta m) - \gamma_m\dot{p} + \xi(t) \tag{3.62}$$

$$\delta\dot{p} = -\omega_m\dot{q} + g_0(m_s\delta m^* + m_s^*\delta m) - \gamma_m\dot{p} + \xi(t) \tag{3.63}$$

In similar manner, substituting Eq. (3.55), Eq. (3.56) and Eq.(3.57) into Eq.(3.47) we get

$$\delta\dot{m} = -(\Delta_m + \kappa_m)(m_s + \delta m) - ig_{mc}(c_s + \delta c) - ig_{mb}(m_s + \delta m)(q_s + \delta q) + \Omega + \sqrt{2\kappa_m}m^{in} \tag{3.64}$$

Form Eq.(3.64) we obtain average value of m_s by setting the derivatives to zero

$$m_s = -\frac{ig_{mc}c_s - \Omega}{(i\Delta_m + \kappa_m + ig_{mb}q)}. \tag{3.65}$$

Substituting Eq.(3.65) into Eq. 3.64, we can easily obtain.

$$\delta\dot{m} = -\left(i\widetilde{\Delta}_m + \kappa_m\right)\delta m - ig_{ma}\delta c - ig_{mb}m_s\delta q + \sqrt{2\kappa_m}m^{in} \tag{3.66}$$

Finally for c_s substitute Eq. (3.55) and Eq. (3.56) into Eq.(3.46) we have

$$\dot{c} = -(\Delta_c + \kappa_c)(c_s + \delta c) - ig_{mc}(m_s + \delta m) + 2Ge^{i\theta}(c_s^* + \delta c^*) + \sqrt{2\kappa_c}c^{in}. \tag{3.67}$$

Again setting the derivatives to zero

$$c_s = \frac{ig_{mc}m_s}{2Ge^{i\theta} - (i\Delta_c + \kappa_c)} \tag{3.68}$$

Substituting Eq.(3.68) into Eq. 3.67, we find that

$$\delta\dot{c} = -(i\Delta_c + \kappa_c)\delta\hat{c} - ig_{mc}\delta\hat{m} + 2Ge^{i\theta}\delta c^* + \sqrt{2\kappa_c}\hat{c}^{in}, \tag{3.69}$$

Thus, for the fluctuation operators, we obtain the linearized quantum Langevin equations as

$$\dot{\delta q} = \omega_b \delta p, \tag{3.70}$$

$$\delta\dot{p} = -\omega_b q + g_{mb}(m_s \delta m^* + m_s^* \delta m) - \gamma_m \dot{p} + \xi(t), \tag{3.71}$$

$$\delta\dot{m} = -\left(i\widetilde{\Delta}_m + \kappa_m\right)\delta m - ig_{mc}\delta c - ig_{mb} m_s \delta q + \sqrt{2\kappa_m} m^{in}, \tag{3.72}$$

$$\delta\dot{c} = -(i\Delta_c + \kappa_c)\delta\hat{c} - ig_{mc}\delta\hat{m} + 2Ge^{i\theta}\delta c^\dagger + \sqrt{2\kappa_c}\hat{c}^{in}. \tag{3.73}$$

3.5 The fluctuation equations of motion of the system

Quadrature fluctuations within a quantum system can be effectively described using the linearized quantum Langevin equations (QLEs). This method is particularly valuable for studying the stability and quantum noise characteristics of the system, providing insights into the behavior of quantum correlations and entanglement between different system components.

We represent the fluctuation operator using quadrature fluctuations in the following manner:

$$f(t)^T = [\delta x_1(t), \delta y_1(t), \delta x_2(t), \delta y_2(t), \delta q, \delta p]$$

with

$$\delta x_1 = \frac{(\delta c + \delta c^\dagger)}{\sqrt{2}}, \tag{3.74}$$

$$\delta y_1 = \frac{i(\delta c^\dagger - \delta c)}{\sqrt{2}}, \tag{3.75}$$

$$\delta x_2 = \frac{(\delta m + \delta m^\dagger)}{\sqrt{2}}, \tag{3.76}$$

$$\delta y_2 = \frac{i(\delta m^\dagger - \delta m)}{\sqrt{2}}. \tag{3.77}$$

and for the corresponding Hermitian input noise operators of the system,we s

$$\delta {x_1}^{in} = \frac{c^{in} + c^{in\dagger}}{\sqrt{2}}, \tag{3.78}$$

$$\delta {y_1}^{in} = \frac{c^{in} - c^{in\dagger}}{i\sqrt{2}}, \tag{3.79}$$

$$\delta {x_2}^{in} = \frac{m^{in} + m^{in\dagger}}{\sqrt{2}} \tag{3.80}$$

$$\delta {y_2}^{in} = \frac{m^{in} - m^{in\dagger}}{i\sqrt{2}}. \tag{3.81}$$

After using Eq. (3.76) and Eq.(3.77) into Eq. (3.71) we get

$$\dot{\delta p} = -\omega_b \delta q - \gamma_b \delta p + i\sqrt{2} g_{mb} \langle m \rangle \delta y + \xi, \tag{3.82}$$

and defining $G_{mb} = i\sqrt{2} g_{mb} \langle m \rangle$, we get

$$\dot{\delta p} = -\omega_b \delta q - \gamma_b \delta p + G_{mb} \delta y + \xi. \tag{3.83}$$

Now, taking the time derivative of Eq. (3.74),we get

$$\delta \dot{\hat{x}}_1 = \frac{(\delta \dot{\hat{c}} + \delta \dot{\hat{c}}^\dagger)}{\sqrt{2}}. \tag{3.84}$$

When we combine Eq. (3.73) with Eq. (3.84), we obtain

$$\begin{aligned} \delta \dot{\hat{x}}_1 = \frac{1}{\sqrt{2}} \Big(&- (i\Delta_c + \kappa_c)\delta \hat{c} - i g_{mc} \delta \hat{m} + 2G e^{i\theta} \delta c^\dagger + \sqrt{2\kappa_c} \hat{c}^{in} \\ &- (-i\Delta_c + \kappa_c)\delta \hat{c}^\dagger + i g_{mc} \delta \hat{m}^\dagger + 2G e^{-i\theta} \delta c + \sqrt{2\kappa_c} \hat{c}^{in\dagger} \Big). \end{aligned} \tag{3.85}$$

Employing the Euler relations

$$e^{i\theta} = \cos\theta + i \sin\theta \tag{3.86}$$

and

$$e^{-i\theta} = \cos\theta - i \sin\theta \tag{3.87}$$

we can express Eq.(3.85) as

$$\begin{aligned} \dot{\delta x_1} =& (-\kappa_c + 2G\cos(\theta)) \frac{(\delta c + \delta c^\dagger)}{\sqrt{2}} + (\Delta_c + 2G\sin(\theta)) \frac{i(\delta c^\dagger - \delta c)}{\sqrt{2}} \\ &+ g_{mc} \frac{i(\delta m^\dagger - \delta m)}{\sqrt{2}} + \sqrt{2\kappa_c} \frac{c^{in} + c^{in\dagger}}{\sqrt{2}} \end{aligned} \tag{3.88}$$

Thus, by comparing Eq. (3.74), Eq. (3.75), Eq. (3.77) and Eq. (3.78) with Eq. (3.88) one can get

$$\dot{\delta x_1} = (-\kappa_c + 2G\cos(\theta))\delta x_1 + (\Delta_c + 2G\sin(\theta))\delta y_1 + g_{mc} \delta y_2 + \sqrt{2\kappa_c} \delta {x_1}^{in} \tag{3.89}$$

Differentiating Eq.(3.75) with respect to time,we find that

$$\delta \dot{\hat{y}}_1 = i \frac{(\delta \dot{\hat{c}}^\dagger - \delta \dot{\hat{c}})}{\sqrt{2}}. \tag{3.90}$$

When we combine Eq. (3.73) with Eqs. (3.90), we obtain

$$\begin{aligned}\delta\dot{\hat{y}}_1 = i\frac{1}{\sqrt{2}}\Big(&-(-i\Delta_c+\kappa_c)\delta\hat{c}^\dagger + ig_{mc}\delta\hat{m}^\dagger + 2Ge^{i\theta}\delta c + \sqrt{2\kappa_c}\hat{c}^\dagger_{\text{in}} \\ &+ (i\Delta_c+\kappa_c)\delta\hat{c} + ig_{mc}\delta\hat{m} - 2Ge^{-i\theta}\delta c^\dagger - \sqrt{2\kappa_c}\hat{c}_{\text{in}}\Big).\end{aligned} \tag{3.91}$$

Inserting Eq.(3.86) and (3.87) in to Eq.(3.91), we obtain

$$\begin{aligned}\dot{\delta y_1} =&(-\Delta_c + 2G\sin(\theta))\frac{(\delta c+\delta c^\dagger)}{\sqrt{2}} - (\kappa_c + 2G\cos(\theta))\frac{i(\delta c^\dagger - \delta c)}{\sqrt{2}} \\ &- g_{mc}\frac{(\delta m+\delta m^\dagger)}{\sqrt{2}} + \sqrt{2\kappa_c}\frac{c^{in}-c^{in\dagger}}{i\sqrt{2}},\end{aligned} \tag{3.92}$$

Thus, by comparing Eq. (3.74), Eq. (3.75),Eq. (3.76) and Eq. (3.79) with Eq. (3.92) one can get.

$$\dot{\delta y_1} = (-\Delta_c + 2G\sin(\theta))\delta x_1 - (\kappa_c + 2G\cos(\theta))\delta y_1 - g_{mc}\delta x_2 + \sqrt{2\kappa_c}\delta {y_1}^{in} \tag{3.93}$$

Following a similar procedure, it can be established that

$$\dot{\delta x_2} = g_{mc}\delta y_1 - \kappa_m\delta x_2 + \Delta_m\delta y_2 - G_{mb}\delta q + \sqrt{2\kappa_m}\delta {x_2}^{in}, \tag{3.94}$$

and

$$\dot{\delta y_2} = -g_{mc}\delta x_1 - \Delta_m\delta x_2 - \kappa_m\delta y_2 + \sqrt{2\kappa_m}\delta {y_2}^{in}. \tag{3.95}$$

Finally, from Eq.(3.70),Eq. (3.83), Eq. (3.89), Eq. (3.93) , Eq. (3.94), and Eq. (3.95) the system's linearized QLE with fluctuation and dissipation components is expressed as:

$$\dot{\delta q} = \omega_m\delta p \tag{3.96}$$

$$\dot{\delta p} = -\omega_b\delta q - \gamma_b\delta p + G_{mb}\delta y + \xi. \tag{3.97}$$

$$\dot{\delta x_1} = (-\kappa_c + 2G\cos(\theta))\delta x_1 + (\Delta_c + 2G\sin(\theta))\delta y_1 - g_{mc}\delta y_2 + \sqrt{2\kappa_c}\delta {x_1}^{in} \tag{3.98}$$

$$\dot{\delta y_1} = (-\Delta_c + 2G\sin(\theta))\delta x_1 - (\kappa_c + 2G\cos(\theta))\delta y_1 - g_{mc}\delta x_2 + \sqrt{2\kappa_c}\delta {y_1}^{in} \tag{3.99}$$

$$\dot{\delta x_2} = g_{mc}\delta y_1 - \kappa_m\delta x_2 + \widetilde{\Delta}_m\delta y_2 - G_{mb}\delta q + \sqrt{2\kappa_m}\delta {x_2}^{in} \tag{3.100}$$

$$\dot{\delta y_2} = -g_{mc}\delta x_1 - \widetilde{\Delta}_m\delta x_2 - \kappa_m\delta y_2 + \sqrt{2\kappa_m}\delta {y_2}^{in} \tag{3.101}$$

The above equations can be written in matrix form as.

$$\dot{u}(t) = Au(t) + n(t) \tag{3.102}$$

where $\mathbf{A}$ is the drift matrix, u(t) is the vector of quadrature fluctuation operators, and $\boldsymbol{n}(t)^T = \left[\sqrt{2\kappa_{c1}}x_1^{in}(t), \sqrt{2\kappa_{c1}}y_1^{in}(t), \sqrt{2\kappa_m}x_2^{in}(t), \sqrt{2\kappa_m}y_2^{in}(t), 0, \xi(t)\right]$ is the column vector of noise sources.

$$\begin{pmatrix} \delta\dot{X} \\ \delta\dot{Y} \\ \dot{\delta x} \\ \dot{\delta y} \\ \dot{\delta q} \\ \dot{\delta p} \end{pmatrix} = \begin{pmatrix} -\kappa_c + 2G\cos\theta & \Delta_c + 2G\sin\theta & 0 & g_{mc} & 0 & 0 \\ -\Delta_c + 2G\sin\theta & -\kappa_c - 2G\cos\theta & -g_{mc} & 0 & 0 & 0 \\ 0 & g_{mc} & -\kappa_m & \widetilde{\Delta}_m & -G_{mb} & 0 \\ -g_{mc} & 0 & -\widetilde{\Delta}_m & -\kappa_m & 0 & 0 \\ 0 & 0 & 0 & 0 & 0 & \omega_b \\ 0 & 0 & 0 & G_{mb} & -\omega_b & -\gamma_b \end{pmatrix} \begin{pmatrix} \delta X \\ \delta Y \\ \delta x \\ \delta y \\ \delta q \\ \delta p \end{pmatrix} + \begin{pmatrix} \sqrt{2\kappa_{c1}}X_{in} \\ \sqrt{2\kappa_{c1}}Y_{in} \\ \sqrt{2\kappa_m}x_{in} \\ \sqrt{2\kappa_m}y_{in} \\ 0 \\ \xi \end{pmatrix} \tag{3.103}$$

All of the informations of the system are extracted from the coefficient matrix A, which is rewritten below.

$$A = \begin{pmatrix} -\kappa_c + 2G\cos\theta & \Delta_c + 2G\sin\theta & 0 & g_{mc} & 0 & 0 \\ -\Delta_c + 2G\sin\theta & -\kappa_c - 2G\cos\theta & -g_{mc} & 0 & 0 & 0 \\ 0 & g_{mc} & -\kappa_m & \widetilde{\Delta}_m & -G_{mb} & 0 \\ -g_{mc} & 0 & -\widetilde{\Delta}_m & -\kappa_m & 0 & 0 \\ 0 & 0 & 0 & 0 & 0 & \omega_b \\ 0 & 0 & 0 & G_{mb} & -\omega_b & -\gamma_b \end{pmatrix}. \tag{3.104}$$

The solution of Eq. (3.102) is

$$u(t) = M(t)u(0) + \int_0^\infty M(s)n(t-s)\,ds, \tag{3.105}$$

where $M(t) = e^{At}$. The system is stable and reaches its steady state when all of the values of A have negative real parts so that $M(\infty) = 0$. The steady state of the quantum fluctuations of the system is a continuous variable (CV) three mode Gaussian state because of the linearized dynamics and the Gaussian nature of the quantum noises. This state is fully represented by a 6×6 Covariance matrix, whose entries are specified as (Jiao et al., 2022).

$$\mathcal{R}_{ij} = \frac{1}{2}\left\langle u_i(t)u_j^\dagger(t') + u_j^\dagger(t')u_i(t)\right\rangle \tag{3.106}$$

where $(i, j = 1, 2, \ldots, 6)$ and $u_i(t) = M(t)u(0) + \int_0^t dt' M(t')n(t-t')$, since $M(t) = \exp(At)$ and as $t \to \infty$ our system is stable $(M(\infty) = 0)$. Therefore

$$\mathcal{R}_{ij} = \left[\frac{\langle u_i(\infty)u_j(\infty) + u_j(\infty)u_i(\infty)\rangle}{2}\right]. \tag{3.107}$$

The steady state Covariance matrix (CM) $\mathcal{R}$ can be achieved by solving the Lyapunov equation

$$A\mathcal{R} + \mathcal{R}A^T = -D. \tag{3.108}$$

With diffusion matrix $D = \text{diag}[k_c(2N_c + 1), k_c(2N_c + 1), k_m(2N_m + 1), k_m(2N_m + 1), 0, \gamma_b(2N_b + 1)]$ defined through

$$\langle n_i(t)n_j(t') + n_j(t')n_i(t)\rangle/2 = D_{ij}\delta(t - t').$$

We use a numerical method to solve the Lyapunov equation for the covariance matrix since it is too difficult to solve analytically.

To evaluate the entanglement between any two modes of the system, we utilize logarithmic negativity, defined as (Plenio, 2005).

$$E_N = \max[0, -\ln(2\eta)],$$

where η denotes the smallest symplectic eigenvalue of the reduced covariance matrix of the two subsystems in question.

4

Result and Discussion

This chapter provides a comprehensive analysis of the entanglement properties of an optical parametric amplifier (OPA) coupled to a magnomechanical system. The numerical results, which measure the corresponding CM using logarithmic negativity, can be used to confirm the entanglement qualities. In light of this, we investigate how the entanglement formation is impacted by the OPA parametric gain .Using the numerical values in the table below, based on our current parameter declarations, we plot graphs to study the entanglement enhancement.

Table 4.1: The experimental parameters for a cavity magnomechanical system used in our numerical simulation (Li et al., 2018).

No	**Physical parameter**	**Symbol**	**Quantity**
1	Frequency of cavity mode	$\frac{\omega_c}{2\pi}$	10GHz
2	Frequency of magnon mode	$\frac{\omega_m}{2\pi}$	10GHz
3	Frequency of mechanical mode	$\frac{\omega_b}{2\pi}$	10MHz
4	Magnon dissipation rate	$\frac{\kappa_m}{2\pi}$	1MHz
5	Cavity dissipation rate	$\frac{\kappa_c}{2\pi}$	1MHz
6	Mechanical damping rate	$\frac{\gamma_b}{2\pi}$	100Hz
7	Magnomechanical coupling rate	$\frac{g_{mb}}{2\pi}$	1MHz
8	Magnon-cavity coupling rate	$\frac{g_{mc}}{2\pi}$	3.2MHz

4.1 Numerical results and discussions

In this section, we will showcase the graph generated in MATLAB, which provides a visual representation of the enhancement in entanglement properties achieved through the optical parametric amplifier's coupling with the magnomechanical system.

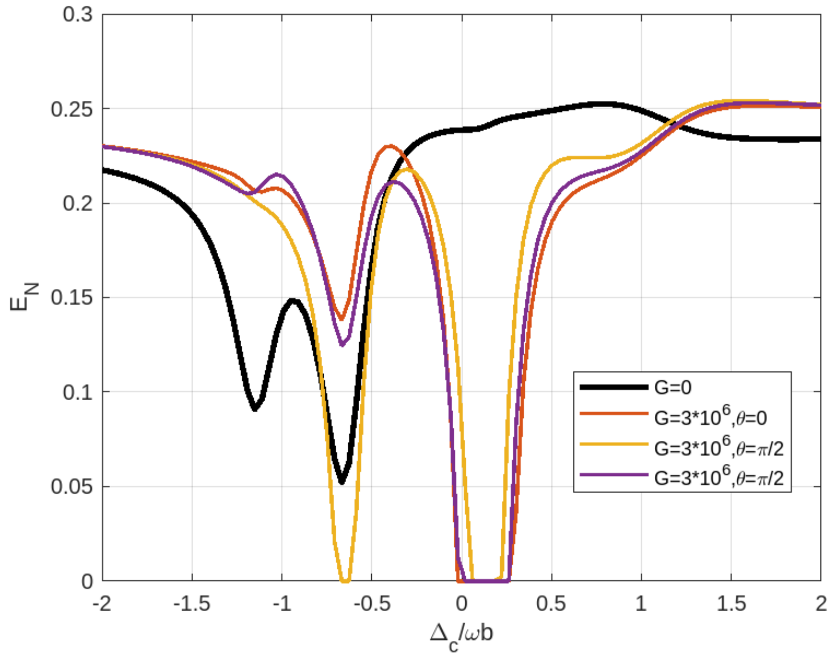

Figure 4.1: Bipartite entanglement involving magnon-phonon modes relative to $\frac{\Delta c}{\omega_b}$. The black curve denotes $G = 0$, while the other curves correspond to $G = 3 \times 10^6\ \mathrm{s}^{-1}$ with three distinct phase settings of θ.

Figure 4.1 investigates the effect of an Optical Parametric Amplifier (OPA) on the bipartite entanglement E_{mb} between magnon and phonon modes within a yttrium iron garnet (YIG) sphere. The graph demonstrates how the normalized detuning Δ_c/ω_b, which indicates the difference between the cavity frequency and the mechanical mode frequency, affects the entanglement.The y-axis quantifies the degree of entanglement using logarithmic negativity E_N, with higher values indicating stronger entanglement.

The baseline condition without the OPA ($G = 0$), shown by the black curve, serves as a reference for comparing the enhanced entanglement conditions induced by the OPA. Upon introducing the OPA, represented by the colored curves at different phase settings ($\theta = 0, \pi/2,$ and π), it becomes evident that the OPA's influence varies with its phase. Although these curves demonstrate that the direct coupling between the magnon and phonon modes within the YIG sphere remains primarily unaffected by the OPA, they also show the OPA's capability to broaden the range of operational conditions under which entanglement is observed. This is highlighted by the shifts in the entanglement peaks across various OPA phases. This extended range is crucial for practical applications, offering more flexibility in experimental setups and potential robustness against fluctuations in system parameters.

The ability to manipulate quantum entanglement through external adjustments like the OPA provides valuable insights into quantum state engineering, paving the way for advancements in quantum computing and communication technologies where controlling entanglement is pivotal.

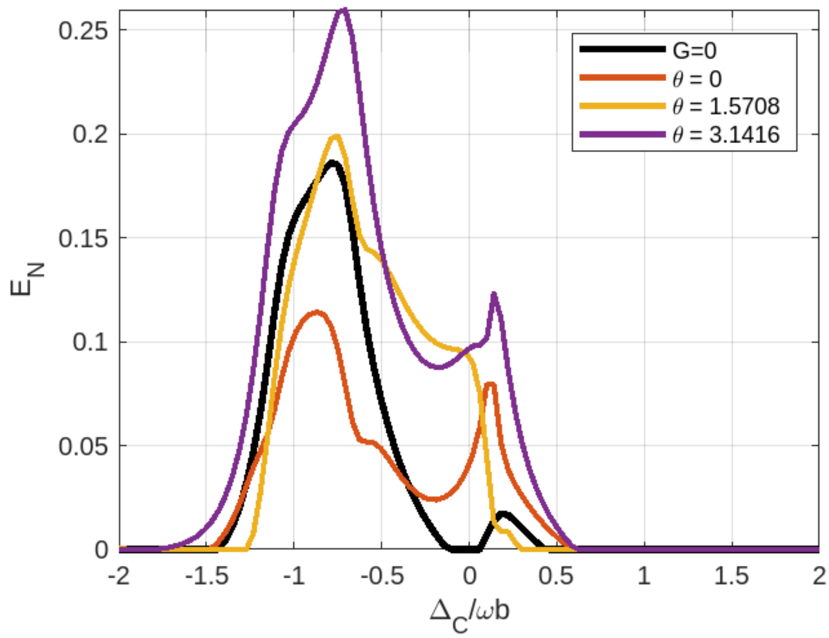

Figure 4.2: Bipartite entanglement among cavity-magnon modes relative to the ratio $\frac{\Delta c}{\omega_b}$. The black curve indicates a scenario where $G = 0$, while the remaining curves represent $G = 3 \times 10^6\,\mathrm{s}^{-1}$, each associated with distinct phase settings of θ.

In Figure 4.2, the diagram presents an exhaustive and detailed visualization of the effect that an Optical Parametric Amplifier (OPA) exerts on the bipartite entanglement E_{cm} between magnon and the cavity modes, as influenced by dimensionless detunings Δ_c/ω_b.The visualization highlights a significant enhancement in the level of entanglement across a broad spectrum of detuning values, facilitated by the incorporation of the OPA. The graph features several curves to denote different conditions, the black curve represents the scenario without OPA ($G = 0$), serving as a baseline for comparison, whereas the colored curves ($\theta = 0$, $\theta = \pi/2$, and $\theta = \pi$) illustrate the entanglement levels under the influence of the OPA at various phase settings. Each color distinctly shows how the OPA's phase affects the entanglement peaks, thereby demonstrating the OPA's role in dynamically tuning the system's quantum interactions for enhanced performance and stability in entanglement driven processes.

The improvement in entanglement can be attributed to the fact that the inclusion of an Optical Parametric Amplifier (OPA) substantially boosts the interaction between cavity and magnon modes by elevating the number of photons in the cavity and modifying the photon dynamics within the cavity mode. OPA creates squeezed states of light, where quantum noise in one variable (quadrature) is reduced below the standard quantum limit while increasing noise in the complementary variable. This property allows the OPA to reduce uncertainty in one variable, increasing the precision of quantum interactions and, thus, improving entanglement.

The phase of squeezing, denoted as θ, plays a crucial role in shaping the characteristics of squeezed light within a given system as you can see it Figure 4.2. This phase determines which quadrature is selectively squeezed. The importance of θ extends beyond simple operational control, it is fundamentally critical for aligning the squeezed state with the specific dynamics of the quantum system in use. By finely adjusting θ, it is possible to specifically tailor the quantum state's behavior, ensuring that the squeezed light interacts optimally with other system components. This precise alignment is essential for fully leveraging the unique properties of squeezed light, enhancing the interaction between light and matter at the quantum level, thereby enabling more precise control over the system's quantum states and their evolution.

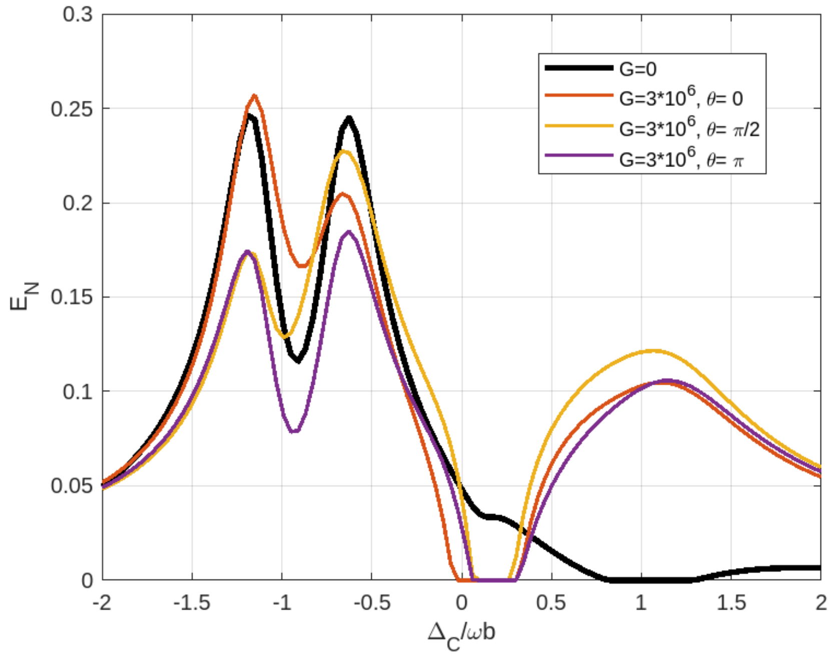

Figure 4.3: Bipartite entanglement among cavity-phonon modes relative to the ratio $\frac{\Delta c}{\omega_b}$. The black curve indicates a scenario where $G = 0$, while the additional curves represent $G = 3 \times 10^6\,\mathrm{s}^{-1}$, each associated with different phase settings of θ.

Figure 4.3 illustrates the bipartite entanglement among cavity-phonon modes over various detuning values. The black curve depicts the condition in the absence of OPA intervention $(G = 0)$, providing a reference point for comparison.The other curves correspond to a gain setting of $G = 3 \times 10^6\,\mathrm{s}^{-1}$ but with three distinct choices of the OPA phase($\theta = 0$, $\theta = \pi/2$, and $\theta = \pi$).The entanglement distribution depicted in Figures 1, 2, and 3, when $(G = 0)$, suggests that the initial entanglement between magnon and phonon is partly redistributed to the subsystems involving the cavity-magnon and cavity-phonon.

Interestingly, Contrary to the usual distribution tendencies, there is a significant increase in phonon-photon entanglement as the cavity detuning approaches to positive mechanical side band. This phenomenon can be attributed to the OPA's impact on the cavity field. As the altered cavity field interacts with the magnon mode, it effectively captures and redistributes the quantum correlations originally present in the light field. This enhancement is a direct result of the OPA's influence, showcasing its effectiveness in altering the quantum landscape to favor specific entanglement pathways.

This result not only highlights the altered entanglement dynamics but also the non-local nature of quantum entanglement. The ability of the entanglement to transfer from one mode to other modes, is particularly indicative of the quantum system's interconnectedness. This extended entanglement, facilitated by the OPA, enhances the overall coherence and quantum interaction capabilities of the system.

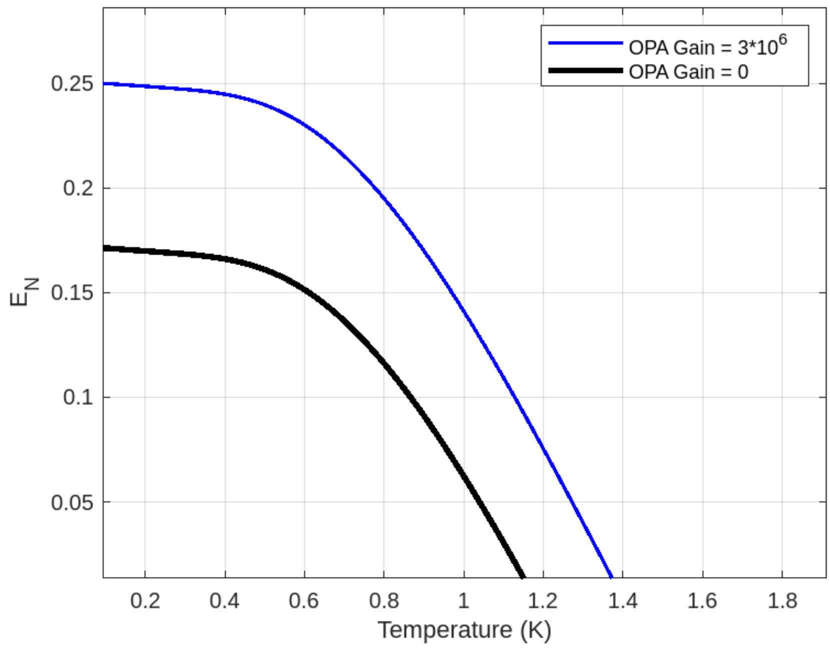

Figure 4.4: Cavity-magnon entanglement relative to temperature both in the presence ($G = 3 \times 10^6, \theta = \pi$) and absence ($G = 0$) of the Optical Parametric Amplifier (OPA). The parameters Δ_c/ω_b and $\tilde{\Delta}_m/\omega_b$ for each curve are finely tuned based on Figure 2.

Notably, the inclusion of the Optical Parametric Amplifier markedly improves the stability of entanglement against temperature variations, as shown in Figure 4.4. This diagram displays cavity-magnon entanglement relative to temperature, contrasting conditions with and without the OPA. The black curve illustrates the degree of entanglement when the OPA is absent, while the blue curve, representing settings where $\theta = \pi$ with the OPA, indicates a substantial enhancement in entanglement at identical temperatures. Consequently, the OPA facilitates the maintenance of strong entanglement even at elevated temperatures.

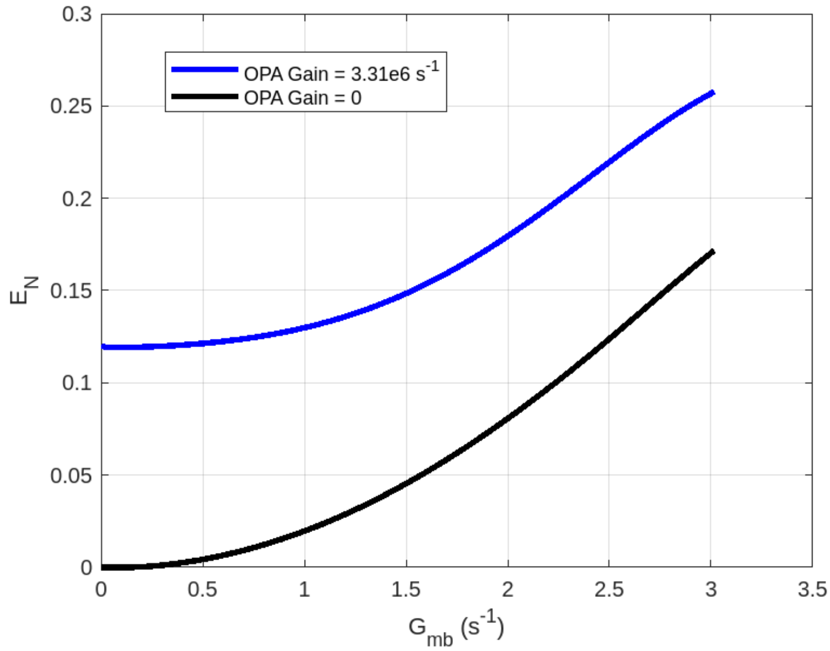

Figure 4.5: Cavity-magnon entanglement in relation to dimensionless magnon-phonon coupling (G_{mb}) is examined in scenarios with ($G = 3 \times 10^6, \theta = \pi$) and without ($G = 0$) the Optical Parametric Amplifier (OPA). The parameters Δ_c/ω_b and $\tilde{\Delta}_m/\omega_b$ are set at $-0.7\omega_b$ and $0.9\omega_b$ respectively.

In Figure 4.5, we illustrate bipartite cavity-magnon entanglement (E_{cm}) as a function of magnon-phonon coupling (G_{mb}) at a fixed value of $\tilde{\Delta}_m = 0.9\omega_b$ and $\tilde{\Delta}_c = -0.7\omega_b$. This comparison is made for both the absence (black curve, $G = 0$) and the presence (blue curve, $G = 3 \times 10^6$, $\theta = \pi$) of an Optical Parametric Amplifier (OPA). When the OPA is absent, the cavity and magnon modes engage in a linear cavity-magnon beam splitter interaction, which is typically unable to create entanglement. Consequently, cavity-magnon entanglement typically requires a finite magnon-phonon coupling to exist.

Remarkably, this requirement is bypassed with the introduction of the OPA.The inclusion of the Optical Parametric Amplifier fundamentally changes the system's dynamics, as evidenced by the blue curve in Figure 4.5. The OPA creates entanglement even when $G_{mb} = 0$, demonstrating its capacity to facilitate robust cavity-magnon entanglement without relying on direct magnon-phonon coupling. This finding highlights the pivotal role of the OPA in optimizing quantum correlations across the system.

5

CONCLUSION AND RECOMMENDATION

5.1 Conclusion

In conclusion, we studied a cavity magnomechanical system featuring a yttrium iron garnet (YIG) crystal within a microwave cavity, specifically designed to amplify quantum interactions. In order to change the statistics of photons within the cavity mode and enhance the cavity's photon occupation number, an Optical Parametric Amplifier (OPA) was also incorporated. We found that incorporating the OPA into the cavity magnomechanical system notably boosted the bipartite entanglement between cavity-magnon and cavity-phonon when the OPA phase was optimally selected. Interestingly, the introduction of the OPA did not substantially impact the magnon-phonon entanglement. This occurred because both the phonon and magnon modes were immediately interconnected inside the YIG sphere, while the OPA only altered the photon statistics. Among the other notable results was the introduction of the Optical Parametric Amplifier (OPA) diminished the requirement for intense magnon-phonon coupling to facilitate cavity-magnon entanglement. Even in the absence of phonon-magnon coupling, we observed substantial cavity-magnon entanglement. Also, the Optical Parametric Amplifier (OPA) increased the system's tolerance to temperature changes. Furthermore, the OPA extended the range of entanglement within the parameter settings, a significant attribute for potential experimental applications.

5.2 Recommendation

In our analysis, the Kerr effect was not considered, primarily due to its significant dependency on both the volume of the sphere and the intensity of the drive field. Given the minimal impact of nonlinear effects in a YIG sphere of 250 micrometers diameter, our model remains robust in a linearized framework. However, for future studies, we recommend investigating the interplay between the Kerr effect and optical parametric amplification (OPA). This approach could potentially unveil new phenomena and enhance the comprehensive scope of the model, offering deeper insights into the dynamics of magnetic and optical interactions.

Research Fund Acknowledgment

This Research Project is funded by Adama Science and Technology University under the grant number ASTU/SM-R/983/24, Adama, Ethiopia.

Bibliography

Abebe, T., Gemechu, N., Gashu, C., Shogile, K., Hailemariam, S., and Adisu, S. (2020). The quantum analysis of nonlinear optical parametric processes with thermal reservoirs. *International Journal of Optics*, 2020:1–11.

Agasti, S. (2020). Theoretical and numerical studies of the dynamics of open quantum systems. *JYU dissertations*.

Amazioug, M., Maroufi, B., and Daoud, M. (2020). Using coherent feedback loop for high quantum state transfer in optomechanics. *Physics Letters A*, 384(27):126705.

Asjad, M., Li, J., Zhu, S.-Y., and You, J. (2023). Magnon squeezing enhanced ground-state cooling in cavity magnomechanics. *Fundamental Research*, 3(1):3–7.

Awschalom, D. D., Du, C. R., He, R., Heremans, F. J., Hoffmann, A., Hou, J., Kurebayashi, H., Li, Y., Liu, L., Novosad, V., et al. (2021). Quantum engineering with hybrid magnonic systems and materials. *IEEE Transactions on Quantum Engineering*, 2:1–36.

Baumgartner, R. and Byer, R. (1979). Optical parametric amplification. *IEEE Journal of Quantum Electronics*, 15(6):432–444.

Brawley, G., Vanner, M., Larsen, P. E., Schmid, S., Boisen, A., and Bowen, W. (2016). Nonlinear optomechanical measurement of mechanical motion. *Nature communications*, 7(1):10988.

Cao, Y., Romero, J., Olson, J. P., Degroote, M., Johnson, P. D., Kieferová, M., Kivlichan, I. D., Menke, T., Peropadre, B., Sawaya, N. P., et al. (2019). Quantum chemistry in the age of quantum computing. *Chemical reviews*, 119(19):10856–10915.

Cerullo, G. and De Silvestri, S. (2003). Ultrafast optical parametric amplifiers. *Review of scientific instruments*, 74(1):1–18.

Chumak, A. V., Kabos, P., Wu, M., Abert, C., Adelmann, C., Adeyeye, A., Åkerman, J., Aliev, F. G., Anane, A., Awad, A., et al. (2022). Advances in magnetics roadmap on spin-wave computing. *IEEE Transactions on Magnetics*, 58(6):1–72.

Cirac, J. I. and Kimble, H. J. (2017). Quantum optics, what next? *Nature Photonics*, 11(1):18–20.

Danaci, O. (2020). *Control of Classical & Quantum Multispatial Modes of Light for Quantum Networks Through Nonlinear Optics and Machine Learning*. PhD thesis, Tulane University School of Science and Engineering.

Darby, M. and Isaac, E. (1974). Magnetocrystalline anisotropy of ferro-and ferrimagnetics. *IEEE Transactions on Magnetics*, 10(2):259–304.

Dias, J. (2020). Quantum repeaters for continuous variables.

Flower, G., Goryachev, M., Bourhill, J., and Tobar, M. E. (2019). Experimental implementations of cavity-magnon systems: from ultra strong coupling to applications in precision measurement. *New Journal of Physics*, 21(9):095004.

Gorbatsevich, A., Kapaev, V., and Kopaev, Y. V. (1994). Magnetoelectric phenomena in nanoelectronics. *Ferroelectrics*, 161(1):303–310.

Hauer, B., Doolin, C., Beach, K., and Davis, J. (2013). A general procedure for thermomechanical calibration of nano/micro-mechanical resonators. *Annals of Physics*, 339:181–207.

Jaeger, G. (2007). *Quantum information*. Springer.

Javanmard, Y., Trapin, D., Bera, S., Bardarson, J. H., and Heyl, M. (2018). Sharp entanglement thresholds in the logarithmic negativity of disjoint blocks in the transverse-field ising chain. *New Journal of Physics*, 20(8):083032.

Jiao, Y.-F., Liu, J.-X., Li, Y., Yang, R., Kuang, L.-M., and Jing, H. (2022). Nonreciprocal enhancement of remote entanglement between nonidentical mechanical oscillators. *Physical Review Applied*, 18(6):064008.

Julsgaard, B., Grezes, C., Bertet, P., and Mølmer, K. (2013). Quantum memory for microwave photons in an inhomogeneously broadened spin ensemble. *Physical review letters*, 110(25):250503.

Kalita, S., Shah, S., and Sarma, A. K. (2022). Significant optoelectrical entanglement and mechanical squeezing in a multimodulated optoelectromechanical system. *Physical Review A*, 106(4):043501.

Kamra, A., Belzig, W., and Brataas, A. (2020). Magnon-squeezing as a niche of quantum magnonics. *Applied Physics Letters*, 117(9).

Kimura, S., Kakihata, K., Sawada, Y., Watanabe, K., Matsumoto, M., Hagiwara, M., and Tanaka, H. (2016). Ferroelectricity by bose–einstein condensation in a quantum magnet. *Nature communications*, 7(1):12822.

Kittel, C. (1949). Physical theory of ferromagnetic domains. *Reviews of modern Physics*, 21(4):541.

Kittel, C. (1958). Interaction of spin waves and ultrasonic waves in ferromagnetic crystals. *Physical Review*, 110(4):836.

Kounalakis, M., Bauer, G. E., and Blanter, Y. M. (2022). Analog quantum control of magnonic cat states on a chip by a superconducting qubit. *Physical review letters*, 129(3):037205.

Kusminskiy, S. V., Tang, H. X., and Marquardt, F. (2016). Coupled spin-light dynamics in cavity optomagnonics. *Physical Review A*, 94(3):033821.

Lachance-Quirion, D., Tabuchi, Y., Gloppe, A., Usami, K., and Nakamura, Y. (2019). Hybrid quantum systems based on magnonics. *Applied Physics Express*, 12(7):070101.

Lachance-Quirion, D., Tabuchi, Y., Ishino, S., Noguchi, A., Ishikawa, T., Yamazaki, R., and Nakamura, Y. (2017). Resolving quanta of collective spin excitations in a millimeter-sized ferromagnet. *Science advances*, 3(7):e1603150.

Lam, P. K. et al. (1998). Applications of quantum electro-optic control and squeezed light.

Lee, E. W. (1955). Magnetostriction and magnetomechanical effects. *Reports on progress in physics*, 18(1):184.

Li, J., Zhu, S.-Y., and Agarwal, G. (2018). Magnon-photon-phonon entanglement in cavity magnomechanics. *Physical review letters*, 121(20):203601.

Liao, C.-G., Xie, H., Shang, X., Chen, Z.-H., and Lin, X.-M. (2018). Enhancement of steady-state bosonic squeezing and entanglement in a dissipative optomechanical system. *Optics Express*, 26(11):13783–13799.

Loudon, R. (2000). *The quantum theory of light*. OUP Oxford.

Marty, G., Combrié, S., Raineri, F., and De Rossi, A. (2021). Photonic crystal optical parametric oscillator. *Nature photonics*, 15(1):53–58.

Osada, A., Gloppe, A., Hisatomi, R., Noguchi, A., Yamazaki, R., Nomura, M., Nakamura, Y., and Usami, K. (2018). Brillouin light scattering by magnetic quasivortices in cavity optomagnonics. *Physical review letters*, 120(13):133602.

Pérez-Arjona, I., Roldán, E., and de Valcárcel, G. J. (2004). Quantum squeezing of optical dissipative structures. *EPL*, 74:247–253.

Plenio, M. B. (2005). Logarithmic negativity: a full entanglement monotone that is not convex. *Physical review letters*, 95(9):090503.

Ruggiero, P., Alba, V., and Calabrese, P. (2016). Entanglement negativity in random spin chains. *Physical Review B*, 94(3):035152.

Sadiek, G. and Kais, S. (2013). Persistence of entanglement in thermal states of spin systems. *Journal of Physics B: Atomic, Molecular and Optical Physics*, 46(24):245501.

Stancil, D. D. and Prabhakar, A. (2009). *Spin waves*, volume 5. Springer.

Tabuchi, Y., Ishino, S., Noguchi, A., Ishikawa, T., Yamazaki, R., Usami, K., and Nakamura, Y. (2015). Coherent coupling between a ferromagnetic magnon and a superconducting qubit. *Science*, 349(6246):405–408.

Teufel, J. D., Li, D., Allman, M. S., Cicak, K., Sirois, A., Whittaker, J. D., and Simmonds, R. (2011). Circuit cavity electromechanics in the strong-coupling regime. *Nature*, 471(7337):204–208.

Vashahri-Ghamsari, S., Lin, Q., He, B., and Xiao, M. (2021). Magnomechanical phonon laser beyond the steady state. *Physical Review A*, 104(3):033511.

Vitali, D., Gigan, S., Ferreira, A., Böhm, H., Tombesi, P., Guerreiro, A., Vedral, V., Zeilinger, A., and Aspelmeyer, M. (2007). Optomechanical entanglement between a movable mirror and a cavity field. *Physical review letters*, 98(3):030405.

Wang, J. (2022). Entanglement in a cavity magnomechanical system. *Quantum Information Processing*, 21(3):105.

Xiang, Z.-L., Ashhab, S., You, J., and Nori, F. (2013). Hybrid quantum circuits: Superconducting circuits interacting with other quantum systems. *Reviews of Modern Physics*, 85(2):623.

Zahn, M. (2006). Derivation of the korteweg-helmholtz electric and magnetic force densities including electrostriction and magnetostriction from the quasistatic poynting's theorems. In *2006 IEEE Conference on Electrical Insulation and Dielectric Phenomena*, pages 186–189. IEEE.

Zhang, C.-y., Li, H., Pan, G.-x., and Sheng, Z.-q. (2016a). Entanglement of movable mirror and cavity field enhanced by an optical parametric amplifier. *Chinese Physics B*, 25(7):074202.

Zhang, X., Zou, C.-L., Jiang, L., and Tang, H. X. (2014). Strongly coupled magnons and cavity microwave photons. *Physical review letters*, 113(15):156401.

Zhang, X., Zou, C.-L., Jiang, L., and Tang, H. X. (2016b). Cavity magnomechanics. *Science advances*, 2(3):e1501286.

Zhou, L., Lin, J., Jing, Y., and Yuan, Z. (2023). Twin-field quantum key distribution without optical frequency dissemination. *nature communications*, 14(1):928.

Zuo, X., Fan, Z.-Y., Qian, H., Ding, M.-S., Tan, H., Xiong, H., and Li, J. (2024). Cavity magnomechanics: from classical to quantum. *New Journal of Physics*, 26(3):031201.